Hybrid Nanofluid squeezing flow with Hall current and non-uniform source/sink

Thesis Submitted By

Maham Rehman

(01-248192-003)

Supervised By

Prof. Dr. M. Ramzan

A dissertation submitted to the Department of Computer Science, Bahria University, Islamabad as a partial fulfillment of the requirements for the award of the degree of

MS (Mathematics)

Session (2019-2021)

Bahria University
Discovering Knowledge

MS-13

THESIS COMPLETION CERTIFICATE

Student's Name: **Maham Rehman** Registration No. **63119** Programme of Study: **MS MATHEMATICS**

Thesis Title: **Hybrid Nanofluid squeezing flow with Hall current and non-uniform source/sink**

It is to certify that the above student's thesis has been completed to my satisfaction and, to my belief, its standard is appropriate for submission for Evaluation. I have also conducted plagiarism test of this thesis using HEC prescribed software and found similarity index at **0%** that is within the permissible limit set by the HEC for the MS/MPhil degree thesis. I have also found the thesis in a format recognized by the BU for the MS/MPhil thesis.

Principal Supervisor's Signature: _____

Date: 15-10-2021 Name: Prof. Dr. Muhammad Ramzan

Bahria University
Discovering Knowledge

MS-14A

Author's Declaration

I **Maham Rehman** hereby state that my MS thesis titled "**Hybrid Nanofluid squeezing flow with Hall current and non-uniform source/sink**" is my own work and has not been submitted previously by me for taking any degree from university Bahria University or anywhere else in the country/world.

At any time if my statement is found to be incorrect even after my graduate the university has the right to withdraw/ cancel my MS degree.

Name of student: **Maham Rehman**

Date: **15-10-2021**

Bahria University
Discovering Knowledge

MS-14B

Plagiarism Undertaking

I, solemnly declare that research work presented in thesis titled "**Hybrid Nanofluid squeezing flow with Hall current and non-uniform source/sink**" is solely my research work with no significant contribution from any other person. Small contribution/ help wherever taken has been duly acknowledged and that complete thesis has been written by me.

I understand the zero tolerance policy of the HEC and Bahria University towards plagiarism. Therefore, I as an Author of above titled declare that no portion of my thesis has been plagiarized and any material used as references is properly referred/cited.

I understand that if I am found guilty of any formal plagiarism in the above titled thesis even after award of MS degree, the university reserved the right to withdraw/revoke my MS degree and that HEC and the University has the right to publish my name on the HEC/University website on which names of students are placed who submitted plagiarized thesis.

Student/ Author's Sign:

Name of the Student**: Maham Rehman**

Dedicated to my exceptional parents and teachers whose tremendous support and cooperation led me to this wonderful accomplishment

Acknowledgments

I am thankful to Almighty ALLAH Who has enabled me to learn and to achieve milestones towards my destination and His beloved Prophet Hazrat Muhammad (ﷺ) Who is forever a constant source of guidance, a source of knowledge and blessing for entire creation. His teachings show us a way to live with dignity, stand with honour and learn to be humble.

My acknowledgment is to my kind, diligent and highly zealous supervisor, Prof. Dr. M. Ramzan, who supported me with his cherished opinions and inspirational discussions. His valuable expertise, comments, suggestions and instructions are most welcome that greatly improved the clarity of this document. I am placing my earnest thanks to Prof. Dr. M. Ramzan. I am so grateful to work under the supervision of such a great person.

My gratitude is to my honourable professors who took me to the apex of my academia with their guidance. In particular, Prof. Dr. Rizwan and Dr. Jafar Hasnain who have always been supportive in all of my course work and kept encouraging me throughout the session in Bahria University, Islamabad Campus. They are the true teachers who have made Mathematics Department of BUIC, a real place of learning.

My intense recognition is to my parents, adored siblings and my husband (for everything) who are always real pillars for my encouragement and showered their everlasting love, care and support throughout my life. Humble prayers, continuing support and encouragement of my family are as always highly appreciated. I also appreciate the moral support of all my friends, Maryam and Noor Us Saba, especially Nazia Shahmir and all PhD scholars who did cooperation up to his best and help me at every step and stage at my research work. Consequently, My all plea is to Allah, the Almighty, the beneficent Whose blessings are always showered upon me via strengthening my wis- dom and bestowed me with the knowledge of what he wants.

Maham Rehman

Bahria University Islamabad, Pakistan

October 2021

Abstract

This study aims to investigate unsteady hybrid nanofluid squeezing flow based engine oil as base fluid, suspended in the midst of two revolving extensible disks with copper (Cu) and Gold (Au) as nanoparticles. Disks are rotating and stretching as different velocities and rates. The intended model is enhanced under the effect of cattaneo-christov(C-C) heat flux and thermal stratification. The influenced of non-uniform heat source/sink is demonstrated in the unique nature of the problem. Relevant similarity transformation method is supplemented for the conversion of partial differential equations into ordinary differential equations. A software, MATLAB function bvp4c is implemented to visualize the model. Sketches portraying impacts on velocities and temperature versus arising parameters are drawn and deliberated well. Moreover, drag force coefficient and heat transfer rate are evaluated for upper and lower disks in tabular form..

TABLE OF CONTENTS

CHAPTER	TITLE	PAGE
	DECLARATION	
	DEDICATION	
	ACKNOWLEDGEMENTS	
	ABSTRACT	
	TABLE OF CONTENTS	
	LIST OF TABLES	
	LIST OF FIGURES	
	NOMENCLATURE	
1.	**Introduction and Literature review**	1
	1.1 Introduction	1
	1.2 Literature review	4
2.	**Preliminaries**	
	2.1 Fluid	9
	2.2 Nanofluid	9
	2.3 Hybrid Nanofluid	9
	2.4 Fluid Mechanics	10
	2.4.1 Fluid Statics	10
	2.4.2 Fluid Dynamics	10
	2.5 Flow	10
	2.5.1 Laminar Flow	10
	2.5.2 Turbulent Flow	10
	2.5.3 Squeezing Flow	
	2.5.4 Unsteady Flow	
	2.6 Viscosity	10
	2.6.1 Dynamic Viscosity	11
	2.6.2 Kinematic Viscosity	11

2.7 Shear Stress 11

2.8 Newton's law of viscosity 12

2.8.1 Newtonian fluids 12

2.8.2 Non-Newtonian fluids 12

2.9 Density 13

2.10 Pressure 13

2.11 Thermal Stratification 14

2.12 Magnetohydrodynamics 14

2.13 Heat Flux 14

2.14 Fourier Law 14

2.15 Cattaneo-Christov Heat flux 15

2.16 Hall current 15

2.17 Heat Transfer Mechanism 15

2.17.1 Conduction 15

2.17.2 Convection 16

2.17.3 Radiation 16

2.18 Chemical reactions 16

2.18.1 Homogeneous reaction 16

2.18.2 Heterogeneous reaction 16

2.19 Mass Conservation Law 17

2.20 Momentum Conservation Law 17

2.21 Energy Conservation Law 18

2.22 Non-dimensional parameters 18

2.22.1 Skin friction Coefficient 18

2.22.2 Nusselt Number 19

2.22.3 Prandtl Number 19

2.22.4 Reynolds Number 19

2.22.5 Schmidt number 19

2.25.6 Thermal relaxation Parameter 20

2.23 Thermal Conductivity 20

2.24 Thermal Diffusivity 20

2.25 Electrical conductivity 20

2.26 Specific Heat Capacity 21

3. Unsteady MHD carbon nanotubes suspended nanofluid with thermal stratification and non-linear thermal radiation 22

3.1 Mathematical formulation 22

3.1.1 Similarity Transformations 26

3.2 Surface drag force coefficient and rate of heat transfer 28

3.3 Results and discussion 30

4. Hybrid Nanofluid squeezing flow with Hall current and non-uniform source/sink 48

4.1 Mathematical formulation 48

4.1.1 Similarity Transformations 52

4.2 Surface drag force coefficient and rate of heat transfer 54

4.3 Results and discussion 55

5. Conclusions and future work 71

5.1 Chapter 3 71

5.2 Chapter 4 71

5.3 Future work 72

Bibliography 73

LIST OF TABLES

Table NO.	TABLE	PAGE
Table 3.1	Thermophysical properties ρ (density), C_p (specific heat), k (thermal conductivity), σ (electrical conductivity) of Ethylene glycol (base fluid) and CNTs (Nanoparticles)	26
Table 3.2	Numerical values of drag force $C_f \operatorname{Re}_x^{1/2}$ versus different values of parameter for SWCNT.	31
Table 3.3	Numerical values of drag force $C_f \operatorname{Re}_x^{1/2}$ versus different values of parameter for MWCNT	33
Table 3.4	Numerical values of heat transfer rate $-\frac{\kappa_{nf}}{k_f}\theta'$ versus different values of parameter for SWCNT.	
Table 3.5	Numerical values of heat transfer rate $-\frac{\kappa_{nf}}{k_f}\theta'$ versus different values of parameter for SWCNT.	
Table 4.1	Thermophysical properties of Cu, Au and Engine oil	43
Table 4.2	Numerical values of drag force k versus different values for hybrid nanofluid by fixing $\phi_1 = 0.02$	48

Table 4.3 Numerical values of drag force $C_f \operatorname{Re}_x^{1/2}$ versus different values for hybrid nanofluid by fixing $\phi_2 = 0.01$ 50

LIST OF FIGURES

Figure No.	Title	Page No.
Figure 3.1	Flow Geometry	23
Figure 3.2	*Change in* $f(\eta)$ vs. Re	33
Figure 3.3	*Change in* $f'(\eta)$ *vs.* Re	33
Figure 3.4	*Change in* $f(\eta)$ *vs.* γ_1	34
Figure 3.5	*Change in* $f'(\eta)$ *vs.* γ_1	34
Figure 3.6	*Change in* $f(\eta)$ *vs.* γ_2	35
Figure 3.7	*Change in* $f'(\eta)$ *vs.* γ_2	35
Figure 3.8	*Change in* $f(\eta)$ *vs.* ϕ	36
Figure 3.9	*Change in* $f'(\eta)$ *vs.* ϕ	36

Figure 3.10	*Change in* $g(\eta)$ *vs.* Re	37
Figure 3.11	*Change in* $g(\eta) vs. M$	37
Figure 3.12	*Change in* $g(\eta)$ *vs.* ϕ	38
Figure 3.13	*Change in* $g(\eta)$ *vs.* γ_2	38
Figure 3.14	*Change in* $g(\eta)$ *vs.* Ω	39
Figure 3.15	*Change in* $g(\eta)$ *vs.* γ	39
Figure 3.16	*Change in* $\theta(\eta)$ *vs.* ϕ	40

Figure 3.17	*Change in* $\theta(\eta)$ *vs.* A_1	40
Figure 3.18	*Change in* $\theta(\eta)$ *vs.* Rd	41
Figure 3.19	*Change in* $\theta(\eta)$ *vs.* s	41
Figure 3.20	*Change in* $\psi(\eta)$ *vs.* K_1	42
Figure 3.21	*Change in* $\psi(\eta)$ *vs.* K_2	42
Figure 3.22	*Change in* $\psi(\eta)$ *vs.* Sc	43
Figure 4.1	*Flow geometry*	49
Figure 4.2	*Change in* $f(\eta)$ *vs.* φ_1	58
Figure 4.3	*Change in* $f'(\eta)$ *vs.* φ_1	58
Figure 4.4	*Change in* $f(\eta)$ *vs.* γ_1	59
Figure 4.5	*Change in* $f'(\eta)$ *vs.* γ_1	59

Figure 4.6 *Change in* $f(\eta)$ *vs.* γ_2 60

Figure 4.7 *Change in* $f'(\eta)$ *vs.* γ_2 60

Figure 4.8 *Change in* $f'(\eta)$ *vs.* Sq 61

Figure 4.9 *Change in* $g(\eta)$ *vs.* ϕ_1 61

Figure 4.10 *Change in* $g(\eta)$ *vs.* m 62

Figure 4.11 *Change in* $g(\eta)$ *vs.* Re 62

Figure 4.12 *Change in* $g(\eta)$ *vs.* M 63

Figure 4.13 *Change in* $\theta(\eta)$ *vs.* Rd 63

Figure 4.14 *Change in* $\theta(\eta)$ *vs.* γ 64

Figure 4.15 *Change in* $\theta(\eta)$ *vs.* Pr 64

Figure 4.16 *Change in* $\theta(\eta)$ *vs.* s 65

Figure 4.17 *Change in* $\theta(\eta)$ *vs.* θ_w 65

Figure 4.18 *Change in* $\theta(\eta)$ *vs.* Sq 66

Figure 4.19 *Change in* $\theta(\eta)$ *vs.* A_3 66

Figure 4.20 *Change in* $\theta(\eta)$ *vs.* B_3 67

Figure 4.21 67

NOMENCLATURE

Acronyms	
Cu	Copper
Au	Gold
Nu	Nusselt number
CC	Cattaneo-Christov
CNTs	Carbon nanotubes
MHD	magnetohydrodynamic
Symbols	
r	Stretching constant
q_w	Heat flux towards wall
p^*	Modified pressure
$u,\ v,\ w$	Velocity components
μ_{hnf}	Dynamic viscosity of nanofluid
μ_{hnf}	Dynamic viscosity of hybrid nanofluid
σ_{nf}	Electrical conductivity of nanofluid
σ_{hnf}	Electrical conductivity of hybrid nanofluid
η	Similarity Variable
B_0	Magnetic field
$(C_p)_{nf}$	Heat capacitance of nanofluid
$(C_p)_{hnf}$	Heat capacitance of hybrid nanofluid
	xiii
ρ_{nf}	Density of nanofluid
ρ_{hnf}	Density of hybrid nanofluid
ρ_{s1}	Density of nanoparticle (Cu)

ρ_{s2}	Density of nanoparticle (Au)
$\frac{dV}{dt}$	Velocity
p	Pressure
τ	Cauchy stress tensor
q_r	Heat flux
∇q	Heat flux gradient
∇T	Temperature gradient
∇V	Velocity gradient
k_f	Thermal conductivity of fluid
k_{nf}	Thermal conductivity of nanofluid
k_{hnf}	Thermal conductivity of hybrid nanofluid
k_{CNT}	Thermal conductivity of carbon nanotubes
k_{s1}	Thermal conductivity of Cu nanoparticle
k_{s2}	Thermal conductivity of Au nanoparticle
k_{bf}	Thermal conductivity of base fluid
ν_{nf}	Kinematic viscosity of nanofluid
ν_{hnf}	Kinematic viscosity of hybrid nanofluid
	xiii
T	Temperature
T_2	Temperature at upper disk
T_1	Temperature at lower disk
a_1, a_2	Stretching rates

ϕ	Nanoparticle volume fraction
ϕ_1	Nanoparticle volume fraction (Cu)
ϕ_2	Nanoparticle volume fraction (Au)
$f(\eta), f'(\eta), g(\eta)$	Dimensional velocities
θ	Dimensionless temperature
$\psi(\eta)$	Concentration
Ω	Rotation parameter
S	Thermal stratification parameter
γ	Thermal relaxation parameter
τ_w	Cauchy stress towards wall
C_f	Skin friction coefficient
Pr	Prandtl number
Re	Local Reynold number
γ_1, γ_2	Stretching parameters
A_1	Unsteadiness parameter
θ_w	Temperature ratio parameter
M	Magnetic moment parameter
Rd	Thermal radiation parameter
δ	Ratio of diffusivity
Sc	Schmidt number
K_1, K_2	Strength measures
c	Positive constant
D_p, D_q	Discharge coefficient

Sq	Squeezing parameter
Q^n	Non-uniform heat
A_3	Space parameter
B_3	Temperature parameter
Subscripts	
f	Fluid
w	Wall
nf	Nanofluid
hnf	Hybrid nanofluid
h	Disk difference

Chapter 1

Introduction and Literature review

1.1 Introduction

Any substance that has the ability to flow under the influence of shear force/stress is termed as 'fluid'. Fluids are of substantial importance in various heat transfer applications since they have the ability to act as heat carriers. Low thermal conductivity serves as a major hindrance in the effectiveness of heat transfer fluids [1]. In order to deal with such constraints, various techniques have been employed in order to improve thermal properties of energy transmission fluids. One of the most renowned methods of augmenting thermodynamic attributes of fluids is to suspend small solid particles including metallic, non-metallic and polymeric particles into the fluids to form slurries. However, large sized suspended particles of μm or mm dimensions may result in severe problems such as clogging and abrasion [1]. This problem hinders the potential efficiency of fluids in various heat transfer applications.

In order to tackle this serious concern, scientists are continuously exploring innovative ways and means in order to augment heat transfer characteristics of conventional fluids. In this respect, most of the recent studies are focused upon utilization of nanoparticles with the purpose to develop efficient nanofluids with improved thermos-physical properties with wide-ranged applications in multiple areas such as in solar water heating, engine cooling, cooling of electronics, improving diesel generator efficiency, lowering temperature of heat exchanging devices, refining heat transfer efficiency of chillers, in nuclear reactors, environment cleaning, biomedicine and food applications [2]. In simple terminology, nanofluids are identified as the dilute suspensions

of nanoparticles (with average diameter less than 100 nm) in basefluid with basic objective of enhancing thermal conductivity of heat transfer fluids. There are multiple factors due to which nanofluids have gained an advantage over the conventional fluids. These include 1) high specific surface area resulting in increased heat transfer surface between particles and fluids, 2) reduction in particle clogging and therefore, system miniaturization, and 3) tunable properties such as surface wettability and thermal conductance, by modulating nanoparticle concentration in base fluid [2].

There are different factors which need to be taken into consideration while deciding on the type of nanomaterials for nanofluid preparation. These parameters constitute chemical stability, toxicity, availability, thermophysical attributes, compatibility with base fluid and cost. Different nanoparticles which have been reportedly utilized for nanofluid preparation comprise copper, silver, zinc, iron, titanium, zinc, magnesium, carbon nanotubes, graphene and diamond. Meanwhile, the base fluids commonly utilized in nanofluid formation include ethylene glycol, water, ethylene glycol–water mixtures and oils [3]. One of the most critical challenges related to commercialization of nanofluid is poor stability which adversely affects its thermodynamic attributes and in turn, the shelf life of the product. This is probably due to the interaction among nanoparticles as well as between particles and the surrounding base liquid. Uniform dispersion of particles in the base fluid is one of the prerequisite for preparation of nanofluids and can greatly impact their thermophysical properties. Nanofluids synthesized from two different approaches possess varying attributes since these are not prepared just as a conventional solid-liquid mixture. Rather, special conditions are required to be present in the suspension such as stability, homogeneity, durability and dispersibility.

Nanofluids can be categorized into two main categories:

1-single material nanofluids in which only a single type of nanoparticles are employed for nanofluid preparation

2-hybrid nanofluids which are designed by suspending two or more nanoparticle types into the base fluid [4]. Encouraging outcomes have been witnessed in case of hybrid nanofluids, since these fluids have demonstrated thermal conductivity much higher than that of commonly utilized single material nanofluids. Hybrid nanofluids are developed either by 1) suspending two or more distinct type of nanomaterials in the base fluid, or 2) by dispersing composite/hybrid

nanoparticles in the base fluid [5]. The uniqueness of hybrid material lies on convergence of physical and chemical characteristics of different materials in a homogeneous phase so as to obtain the final product with remarkably favorable and upgraded physicochemical properties, not existent in the individual components. Due to the synergistic effect of individual constituents, hybrid nanofluids are believed to possess enhanced rheological and heat transfer characteristics. For that reason, researchers are continuously exploring synthesis, heat transfer and thermo-physical attributes and fluid flow characteristics of hybrid nanofluids.

In recent years, nanofluids have been proposed as highly feasible heat transfer fluids with much improved performance compared to conventional heat transfer slurries currently employed in applications involving thermal management. Various researches have been conducted in this regard with successful outcomes. The augmented thermal properties of nanofluids would result in their broad ranged applicability in multiple dimensions for instance cooling of engines, electronic apparatus, nuclear reactors, automotive, solar collectors and such others. The most crucial step in preparation of thermally efficient nanofluids is to carefully optimize their synthesis parameters for creating stable suspension of nanomaterials in the base fluid. Varying combinations of nanomaterials and fluids are designed depending upon the requirements in a specific application. Nanofluids can be considered as highly desirable, next generation a liquid coolant if they possess the following attributes [6],

- Thermal conductivity surpassing those of conventional solid/liquid suspension.
- Temperature-dependent thermal conductivity
- Substantial rise in critical heat flux in boiling heat transfer

Several studies have demonstrated that heat transfer attribute of nanofluids is a function of nanoparticle loading in the base fluid. A substantial increase of 30% was witnessed in the thermal conductivity of water after addition of 4.3 percentage volume of Al_2O_3 nanoparticles [7]. However, a similar study reported only 15% increase in thermal conductivity of water under similar conditions [8]. The dissimilarity in outcomes of both studies was accredited to the difference in the average nanoparticle size in two sets of samples.

Dependence of thermal conductivity of nanoparticles over a considerable temperature range is another attractive feature of nanofluids since this property makes them favorable for applications at elevated temperatures. In a recent study, two-to-four fold increase in thermal conduc-

tivity was observed in nanofluid systems over a temperature range of 20-50°C [9]. In convective thermal transfer in nanofluids, heat transfer coefficient depends on many other factors besides thermal conductivity such as density, specific heat and dynamic viscosity of nanofluid. Researchers have observed that nanofluids have decreased viscosities when nanoparticles are more dispersed. It was also inferred that viscosity of nanofluid correlates directly with the method used to stabilize and disperse the nanoparticle suspension.

Stability of nanofluids is the essential parameter for undisrupted functioning of thermal system. Preparation of stable nanofluids comes forward as a key challenge for researchers due to the strong cohesive and Van der Waal forces among nanoparticles. These forces lead to the agglomeration of nanoparticles which in turn results in the agglomeration of hybrid nanofluids, prompting them to lose their heat transferring potential. This is owing to the reduction in Brownian movement of nanoparticles. Nanofluids stability relies upon two basic principles i.e. Diffusion Principle and Zeta Potential Principle. Diffusion principle states that nanoparticles are dispersed into the fluid medium by electric double layer repulsion. Meanwhile, zeta potential principle states that divergence of zeta potential of nanofluid from isoelectric point results in strong repulsive forces among nanoparticles, and thus reduced agglomeration. Variety of methods have been reported in literature to lessen the agglomeration, some of which are 1) addition of surfactants, 2) maintaining control of pH value for electrostatic stabilization, and 3) ultrasonic vibration [6].

Although most of the characteristics of hybrid nanofluids are much similar to those of mono-nanofluids; it is believed that hybrid nanofluid may possess augmented thermal, hydrodynamic and rheological attributes because of the synergistic effect of nanoparticles. Metallic nanoparticles such as Copper, Aluminum and Silver etc. possess higher thermal conductivities but are usually unstable and reactive [10]. These nanoparticles are hybridized with metal or ceramic oxides with a purpose to develop stable and efficient hybrid nanofluids. Metallic nanoparticles form a layer on metal/ceramic oxide particle surface and develop thermal interfaces between boundaries of composite nanoparticles and base fluid, thereby resulting in thermal conductivity augmentation [10].

1.2 Literature review

Nanofluids are continuously being explored for their heat transfer applications. Since most of the machining processes involve increased friction and high temperature surroundings, there is a huge demand of a suitable coolant for such systems. Nanofluids have recently been employed for this purpose due to their advanced thermophysical characteristics. Different types of nanomaterials are added into the base fluids for acquiring efficient nanofluids. Copper and alumina are two most commonly utilized and economical nanoparticles which are being used for preparation of nanofluids. Thermal conductivity of nanofluid comprising Cu, CuO and Al_2O_3 nanoparticles was investigated using two different base fluids i.e. H_2O and HE-200 oil. Both types of hybrid nanofluids demonstrated 60 percentage improvement in the thermal conductivity with the addition of only 5 percent volume of nanoparticles [11]. Another study revealed 20 percent increase in thermal conductance of nanofluid prepared by addition of 4 percent CuO nanoparticles in ethylene glycol base fluid [8]. Researchers have observed that high specific surface area with reduced size of nanomaterials is one of the determining factors in augmenting the thermal conductivity of nanofluids. In a study carried out by Xie and coworkers [12], effect of different parameters was investigated upon thermal conductivity of nanofluids. These included specific surface area of dispersed nanoparticles (Al_2O_3), pH value of suspension, crystalline phase of solid phase and thermal conductivity of base fluid. It was observed that thermal conductivity of nanofluid was directly dependent upon specific surface area of nanoparticles and also upon the difference between pH value and isoelectric point of nanoparticles. On the contrary, the crystallite phase of nanomaterials did not inflict any obvious impact upon thermal conductivity of nanofluid suspension.

Nanofluids containing carbon nanotubes have exhibited largest increase in thermal conductivity of base fluids compared to rest of nanomaterials. Carbon nanotubes form an entangled, immobile fiber network due to which they impart polymer composite like effect during thermal transport of fluid suspension. Biercuk et al. reported used single-walled carbon nanotube-polymer epoxy composite for the first time and indicated 125percent enhanced thermal conductivity at 1% (by weight) loading [13]. Likewise, another study by Choi and co. explored thermal conductance of carbon nanotubes in oil suspensions, and reported 160% augmentation upon 1% loading [14].

A number of researchers have suggested that enhanced thermal conductivity of nanofluids can be accredited to the hydrodynamic effects of Brownian motion of nanoparticles. According to the scientists, each Brownian particle has the ability to generate a long velocity field in the surrounding fluid, similar to that existent around a particle moving with constant velocity. The capability of huge volumes of fluids comprising nanomaterials to carry significant amount of thermal energy is attributed to large thermal conductivity surges of nanofluids [15]. Some of the probable reasons suggested for upgraded thermal conductivity of nanofluids were suggested by Xuan and Li [16], which included 1) increased surface area because of the suspended nanoparticles, 2) enhanced thermal conductivity of fluid, 3) the interaction among suspended particles, the strengthened turbulence of the fluid, as well as, 4) the dispersion of nanoparticles.

Hybrid nanofluids are considered as the advanced category of nanofluids whereby the main objective is to acquire enhanced thermo-physical characteristics compared to the single material nanofluids. Heat transfer characteristics of hybrid nanofluids have been explored by number of researchers. Cu-TiO_2/water hybrid nanofluid was prepared and investigated for its thermo-physical attributes. Results revealed that heat transfer parameters comprising heat transfer coefficient, convective heat transfer coefficient and nusselt number (ratio of convective to conductive heat transfer across a boundary) were augmented by 52%, 68% and 49% respectively at 1% volume of nanofluid [17]. Another study reportedly investigated thermal efficacy of Ag-Al_2O_3/H_2O hybrid nanofluid and found 148% increase in convective heat transfer coefficient at 3% volume of nanofluid [18]. It has also been witnessed that pressure drop and friction factor of hybrid nanofluids also increases proportionally with nanocomposite volume fraction mainly because of the density gradients and viscous forces. The viscosity of hybrid nanofluids experiences substantial increase due to the development of nano-clusters and rearrangements of hybrid nanomaterial with primary nanoparticles. Studies have reported higher pressure drop and friction factor in case of hybrid nanofluid compared to the base fluid. The probable justification for this might be that high concentration of hybrid nanoparticles in base fluid results in magnification of viscous and inertial forces which in turn promotes the friction factor. Further, pressure drop also gets increased with the increase in volume concentration as nanofluid density escalates at higher concentrations [19]. It was also observed that hybridization of copper nanoparticle with alumina results in the development of nanoclusters with amplified hydrody-

namic diameter of constituent nanoparticles which is responsible for increased relative viscosity and hence, greater friction factor compared to the mono-nanofluid or base fluid [20].

At the present, squeezing flow of hybrid nanofluids between two parallel disks is of considerable attention among scientific community. Squeezing flow is generated due to the movement of two plates towards each other. The original concept of squeezing flow was initially presented by Stefan in 1874 who was the first to do foundational work regarding squeezed flows under lubrication assumption [21]. This area has gained much interest recently because of the rising applications of nanofluid squeezed flow in manufacturing and industrial fields such as in lubrication, polymer processing, food processing, compression, metal molding, etc.[22]. Muhammad and coworkers performed comparative analysis for melting heat transfer in squeezing flow of basefluid i.e. water, nanofluid comprising carbon nanotubes and water, and hybrid nanofluid constituting carbon nanotubes, copper oxide and water. Heat transfer parameters including entropy production rate, bejan number, velocity and temperature revealed hybrid nanofluid as the most efficient fluid compared to basefluid (water) and mono-nanofluid (carbon nanotubes).

Two-dimensional magneto-hydrodynamic (MHD) squeezing flow between parallel plates with reference to Homotopy perturbation solution was investigated by Siddiqui and co. [23]. Similar problem was discussed by Domairry and Aziz for exploring the squeezing flow between parallel disks [24]. Recently, mass and heat transfer for squeezing flow between parallel plates was explored by Mustafa et al. [25] by means of homotopy analysis method (HAM).

Rotating flow of electricity conducting nanofluids under the influence of magnetic field is of considerable importance due to its applicability in various industries. If ionized fluid of reduced density is under the influence of strong magnetic field, fluid conductivity falls and consequently, free spiraling of ions around magnetic field lines induces current parallel to the magnetic or electric field in it. This induced current is termed as 'Hall Current'. Effect of hall current has been studied by a number of researchers. Hall current flow was investigated over a stretching surface by Sarojamma and coworkers [26]. Hall Effect in magneto hydrodynamics (MHD) flow of nanofluids was explored in a rotating permeable channel [27]. Fluid flow under Hall Effect was also investigated in case of hybrid nanofluid constituting Cu and CuO nanoparticles with H_2O as basefluid. It was observed in the study that shape of nanoparticles has a profound impact upon fluid flow with platelet shaped nanostructures exhibiting better fluid flow compared to brick

shaped nanoparticles which showed better temperature efficacy [28]. Another study focused upon Cu/Al_2O_3 based hybrid nanofluid in which hybrid nanofluid was observed with increased heat transfer rate under hall current effect over an unsteady rotating disk. Velocity of the fluid was also found decreased with enhanced magnetic parameter whereas temperature was found elevated [29].

In another study conducted by Gull et al, hybrid nanofluid flow was investigated consisting of Cu and Al_2O_3 nanoparticles under the influence of hall and ion slip effect combined with non-uniform source/sink. Thermal performance of Cu nanoparticles was found greater as compared to alumina nanoparticles. Temperature of nanofluid was increased proportionally to the strength of magnetic field. On the contrary, partially ionized nanofluids have lower temperature because of the collision of ions and electrons [30]. Another study investigated the impact of non-uniform heating on thermal transport characteristics for nanofluid convective flow. It was observed that average heat transfer rate was greater in case of non-uniform asymmetric heating compared to uniform heating [31].

Until recently, there has been no research focused upon Copper/Gold nanofluid. Henceforth; this study would prove to be one of its kinds to discuss the squeezing flow pattern of Cu/Au nanofluids with Hall current and non-uniform source/sink.

Chapter 2

Preliminaries

This chapter consists of certain perceptions, definitions and fundamental laws.

2.1 Fluid

When a shear stress or external force is applied to a fluid, it disperses constantly. Fluids include liquids, gases, and plasmas.

2.2 Nanofluid

A nanofluid is a fluid in which nanometer-sized particles embedded in a base fluid create a colloidal nanoparticle solution.This is made by combining a low-thermal-conductivity base fluid with high-thermal-conductivity solid nanoparticles, resulting in nanofluids with a higher transfer characteristic than base fluids.The nanoparticles used in nanofluids are typically made of metals, oxides, carbides, or carbon nanotubes, while the base fluids include water, ethylene glycol, and oil

2.3 Hybrid-nanofluid

A hybrid nanofluid is a form of nanofluid that has a mixture of different types of nanoparticles suspended in a base fluid.

2.4 Fluid mechanics

It is a branch of physics in which we study of fluid behavior (liquids, gases, blood, and plasmas) at rest and in motion.

2.4.1 Fluid statics

It's a branch of fluid mechanics concerned with the behaviour of fluid particles when they are at rest.

2.4.2 Fluid Dynamics

It is a branch of fluid mechanics that studies the behaviour of moving fluid particles.

2.5 Flow

A flow is a substance that deforms in a consistent manner when subjected to various forces.

2.5.1 Types of flow

There are two different ways to describe the flow:

2.5.2 Laminar flow

Fluid particles move along well-defined routes or layers of fluid, all of which are straight,parallel and do not cross each other.

2.5.3 Turbulent flow

Fluid particles move along well-defined routes or layers of fluid, all of which are straight,parallel and do not cross each other.

2.5.4 Squeezing flow

A flow in which a substance is distorted as it approaches two parallel or nearly parallel boundaries. Squeezed flows are expected to be unstable and discordant due to its ability to change

form.

2.5.5 Unsteady flow

A steady flow occurs when the amount of liquid flowing per second through any portion remains consistent.

2.6 Viscosity

The viscosity of a fluid is a measure of the fluid's internal resistance to motion or deformation. In everyday terms viscosity is "thickness" or "internal friction of fluid.

It is divided into two classes:

2.6.1 Dynamic viscosity

Dynamic viscosity is a measure of internal resistance. Dynamic viscosity is the tangential force per unit area required to move one horizontal plane with respect to an other plane at an unit velocity. it is defined as

$$\mu = \frac{(Shear\ stress)}{(Gradient\ of\ velocity)},$$

$$\mu = \frac{(\tau_{yx})}{(du/dy)}. \tag{2.1}$$

A unit of μ is (kg/m.s) in S.I units having dimension [M/LT].

2.6.2 Kinematic viscosity

It is defined as ratio of dynamic viscosity μ to density ρ. it is defined as

$$\nu = \frac{Dynamic\ viscosity}{Fluid\ density},$$

$$\nu = (\mu/\rho), \tag{2.2}$$

It's unit is m^2/s having dimension $[L^2/T]$.

2.7 Newton's law of viscosity

Newton's law of viscosity describe the relation of shear stress and velocity gradiant. It states that shear stress is directly propotional to velocity gradiant.

Mathematically,

$$\tau_{yx} \propto (du/dy), \tag{2.3}$$

or

$$\tau_{yx} = (\mu)(du/dy), \tag{2.4}$$

in witch τ_{yx} indicate the shear stress appliedon the fluid's element and μ indicate the proportionality constant.

2.8 Shear stress

Shear stress is the drag force per unit area imposed by a fluid in motion on a solid boundary in parallel to the direction of the fluid in motion. Shear stress is measured in Pascal(Pa).

2.8.1 Newtonian fluids

Newtonian fluid is defined as a fluid that obeys Newton's viscosity law.Newtonian fluid has constant viscosity at fixed temperature and different shear rates.The relationship between shear stress τ_{yx} and shear rate (du/dy) is linear.Newtonian fluids include water, oil, glycerin, and other similar substances.

2.8.2 Non-Newtonian fluids

Newtonian fluid is defined as a fluid that does not obeys Newton's viscosity law. Non-Newtonian fluid viscosities vary at different shear rates.They have nonlinear relation between shear stress

τ_{yx} and shear rate (du/dy). Non-Newtonian fluids include toothpaste, cosmetics, butter and etc.

Mathematically, it is written as:

$$\tau_{yx} \propto (\frac{du}{dy})^N, N \neq 1,$$

$$\tau_{yx} = (K)(\frac{du}{dy})^N. \tag{2.5}$$

Equation(2.5) is change into Newton's law of viscosity when $K = \mu$, and $N = 1$

$$\tau = (\mu)(\frac{du}{dy}), \mu = (K)(\frac{du}{dy})^{(N-1)}. \tag{2.6}$$

2.9 Density

The ratio of mass of substance/object to its volume is called density. Mathematically, it is stated as:

$$\rho = (\frac{m}{V}). \tag{2.7}$$

Its unit iskg/m^3 with dimensions$[M/L^3]$.

2.10 Pressure

The amount of force F applied per unit area A is called pressure. Mathematically,

$$P = (F/A). \tag{2.8}$$

Its unit is N /m.

2.11 Thermal Stratification

The emergence of two separate layers of water of different temperatures within a body of water is referred to as thermal stratification.The colder, heavier water settle at bottom due to difference in temperature occurs while hot and lighter water floats over upper surface of water.

2.12 Magnetohydrodynamics(MHD)

The study of the dynamics of electrically conducting fluids is known as magnetohydrodynamics (MHD). The term magnetohydrodynamic comes from the words magneto, which means magnetic field, hydro, which means liquid, and dynamic, which means movement. Plasmas, liquid metals, and salt water or electrolytes are examples of such fluids.

2.13 Heat flux

The flow of energy per uni area and time is called heat flux. The heat flow is the measurement of the energy transfer, which is caused by a temperature difference and leads to the temperature balance between substances. Mathematically

$$q = -k(\nabla T). \tag{2.9}$$

In which q is heat flux, k denotes material conductivity and ∇T shows temperature gradient.Its unit in S.I is W/sq.m^2.

2.14 Fourier Law

According to Fourier's law, the area at right angles to the gradient through which heat flows is proportional to the negative gradient of temperature and the time rate of heat transfer.

$$q = -k(\nabla T). \tag{2.10}$$

q is local heat flux density

k shows material's conductivity

∇T denotes temperature's gradient

2.15 Cattaneo-Christov heat flux

It is adaptation of Fourier's law by two mathematicians Cattaneo and Christov. Mathematicaly, it is stated as:

$$q + \lambda_1(q_t + V.\nabla_q - q.\nabla V + (\nabla.V)_q) = -k\nabla T. \tag{2.11}$$

2.16 Hall current

When an electrical current passes through a sample placed in a magnetic field, a potential proportional to the current and to the magnetic field is developed across the material in a direction perpendicular to both the current and to the magnetic field is called Hall current.

2.17 Heat transfer Mechanism

A mechanism that transport energy and entropy from one position to another. It include thermal radiation, convection and conduction.

2.17.1 Conduction

Conduction is heat transfer that occurs within a material due to molecular motion without the material moving as a whole.

Higher-speed particles will collide with slower particles, resulting in a net energy transfer to the slower particles.

$$q = -kA\nabla T = -kA(\frac{dT}{dx}), \tag{2.12}$$

Negative sign indicates flow from higher to lower region. where q denotes the heat transfer, A is area of surface, k the thermal conductivity.

2.17.2 Convection

Heat is transferred via convection when a heated fluid, such as air or water, is forced to flow away from the source of heat, carrying energy with it.

$$q = -HA\nabla T, \tag{2.13}$$

2.17.3 Radiation

The emission or transmission of energy in the form of waves or particles across space or a material medium is known as radiation. Radiation is determined by the Stefan-Boltzmann law of radiation:

$$q = \sigma e A \left(\nabla T\right)^4, \tag{2.14}$$

Where q denotes the heat transfer, e for emissivity of system, σ for constant Stephen-Boltzmann, A for area and $(\nabla T)^4$ for the temperature difference between two systems fourth power.

2.18 Chemical reactions

We grouped the chemical reactions in two types:

2.18.1 Homogeneous reaction

A reaction that occur uniformly through a given phase or a reaction that occur in one phase is called homogeneous reaction. Some examples of homogeneous reactions are air, dishwashing liquid,mixture of sugar and water.

2.18.2 Heterogeneous reaction

A chemical reactions in which the reactants are two or more phase components is called hetrogeneous reaction, for example the reaction of metals with acids, the electrochemical changes that occur in batteries and electrolytic cells.

2.19 Mass conservation law

This law states that in any isolated system, the mass will remain constant. It is also known as equation of continuity. Mathematically

$$(\frac{\partial \rho}{\partial t}) + (\nabla.V)\rho + \rho(\nabla.V) = 0. \tag{2.15}$$

or

$$(\frac{\partial \rho}{\partial t}) + \nabla.(\rho V) = 0. \tag{2.16}$$

Where,

ρ is density

$(\frac{\partial \rho}{\partial t})$ is substance time derivative

V is velocity of fluid

For steady flow Eq.(2.16) convert to:

$$\nabla.(\rho V) = 0. \tag{2.17}$$

For incompressible flow Eq.(2.17) becomes:

$$(\nabla.V) = 0. \tag{2.18}$$

2.20 Momentum conservation law

This law says that in a closed system, the entire linear momentum stays unchanged. Mathematically,

$$\rho(\frac{DV}{Dt}) = div\tau + \rho b, \tag{2.19}$$

$\rho(\frac{DV}{Dt})$ is represents an internal force, $div\tau$ is represenst surface force and ρb is represents body force,where b for body force and τ for Cauchy stress tensor defined as:

$$\tau = -PI + \mu A_1, \tag{2.20}$$

where

$$A_1 = gradv + (gradv)^t. \tag{2.21}$$

2.21 Energy conservation law

This law asserts that all energy in a closed system is conserved. This law is also known as energy eqaution. Mathematically:

$$(\rho C_p)_f(\frac{DT}{Dt}) = \tau.L^* - divq + \rho D_E, \tag{2.22}$$

where

$$q = -k\nabla T, \tag{2.23}$$

$$L^* = \nabla V, \tag{2.24}$$

$$\tau = -PI + \mu A_1, \tag{2.25}$$

$$A_1 = L^* + L^{*T},$$

2.22 Non dimensional parameters

2.22.1 Skin friction coefficient (C_{fr})

In boundary-layer flows, the skin friction coefficient is an important dimensionless parameter. It indicates the percentage of the local dynamic pressure, that is perceived as shear stress on the surface. It occurs between liquid and dense surface, reducing fluid flow's rate. Mathematically, it is written as:

$$C_{fr} = \frac{(\tau_w)}{(1/2)(\rho\nu^2)}. \tag{2.26}$$

2.22.2 Nusselt number (Nu)

The Nusselt number is a dimensionless number used to describe the ratio of the thermal energy convected to the fluid to the thermal energy conducted within the fluid. Mathematically

$$Nu_x = \frac{(h^* \triangle T)}{(k_f \triangle T/l)}, \tag{2.27}$$

$$Nu_x = (h^* l)/(k_f). \tag{2.28}$$

2.22.3 Prandtl number (Pr)

The ratio of momentum diffusivity to heat diffusivity is known as the Prandtl number. It is a dimensionless number. Mathematically

$$Pr = \frac{\nu_f (\rho C_p)_f}{(k_f)}. \tag{2.29}$$

2.22.4 Reynolds number (R_e)

Reynolds number is a non-dimensional number that represents the ratio of inertial forces to viscous forces and is a useful statistic for determining whether a flow will be laminar or turbulent. A low Reynolds number implies laminar flow, which is characterised by viscous effects, whereas a high Reynolds number suggests turbulent flow, which is characterised by inertial effects. Mathematically

$$R_e = \frac{Inertial forces}{Viscous forces},$$

$$R_e = (\rho \nu d/\mu). \tag{2.30}$$

2.22.5 Schmidt number(Sc)

The Schmidt number is a dimensionless number that equals the ratio of momentum diffusivity (kinematic viscosity) to mass diffusivity (mass diffusivity).

$$Sc = (\frac{\mu}{\rho D_m}) = \frac{\nu}{D_m}. \tag{2.31}$$

2.22.6 Thermal relaxation parameter(γ)

It is dimensionless widely used parameter for calcuating amount of time it takes for heat conduction.

2.23 Thermal conductivity (k)

By inducing a per unit thermal gradient, the time rate of steady-state heat flow through a body of per unit area. Thermal conductivity is the ability of a material to conduct heat. Mathematically

$$k = ((Qd)/(A\triangle T)). \tag{2.32}$$

2.24 Thermal diffusivity (α)

At constant pressure, thermal diffusivity is defined as thermal conductivity divided by density and specific heat capacity. It quantify the rate at which heat is transferred from a hot to a cold side of a substance or material. Mathematically

$$\alpha = (k/(\rho C_p)). \tag{2.33}$$

2.25 Electrical conductivity(σ)

The electrical conductivity of a material is a measurement of how well it conducts electricity. Electrical conductivity and electrical conductance are inextricably linked. The substance's electrical conductivity is a property of the material and is given by

$$\sigma = (h/(AR)). \tag{2.34}$$

Where A is cross sectional area R, is electrical resistence and h is distance.

2.26 Specific heat capacity (C_P)

The quantity of heat that must be given to a system's unit mass in order to raise (or lower) its temperature by 1K is called specific heat capacity. Mathematically it is written as:

$$C_p = (\frac{Q}{m\nabla T}). \tag{2.35}$$

Chapter 3

Unsteady MHD carbon nanotubes suspended nanofluid with thermal startification and non-linear thermal radiation

In this chapter, Hall current and cattaneo-christov(C-C) heat flux impact nanofluid magneto-hydrodynamic(MHD) flow in Ethylene glycol (C2H6O2), which is employed as the base fluid. The flow is in the centre of two revolving extensible discs suspended using carbon nanotubes (CNTs) as nano-particles. The particular nature of the problem presented is demonstrated by the inclusion of thermal stratification, homogeneous-heterogeneous reactions and nonlinear thermal radiation. The governing systems of PDE's have been transformed into a set of ordinary differential equations by using sufficient similarity transformations and boundary layer strategy. For the resulting equations, the bvp4c approach is used.

3.1 Mathematical formulation

Represented a time-dependent MHD flow with Ethylene glycol ($C_2H_6O_2$) as a base variable,using the two types of nano-particles single-wall (SWCNTs) and multi-wall (MWCNTs)

carbon nanotubes. Heat transfer through the base fluid and field current effect is placed in a thermally segregated medium.The flow is known among two simultaneous disks having the length h. The disks are stretched at the rate $a_1$and a_2,with angular velocities Ω_1 and Ω_2 about its axis. The steady state velocity is expressed as $V[u(r,\theta), v(r,\theta), w(r,\theta)]$ with (u, v, w) are velocity components in addition to (r, θ, z) directions. T_1 and T_2 are tenperature of lower and upper disk respectively.

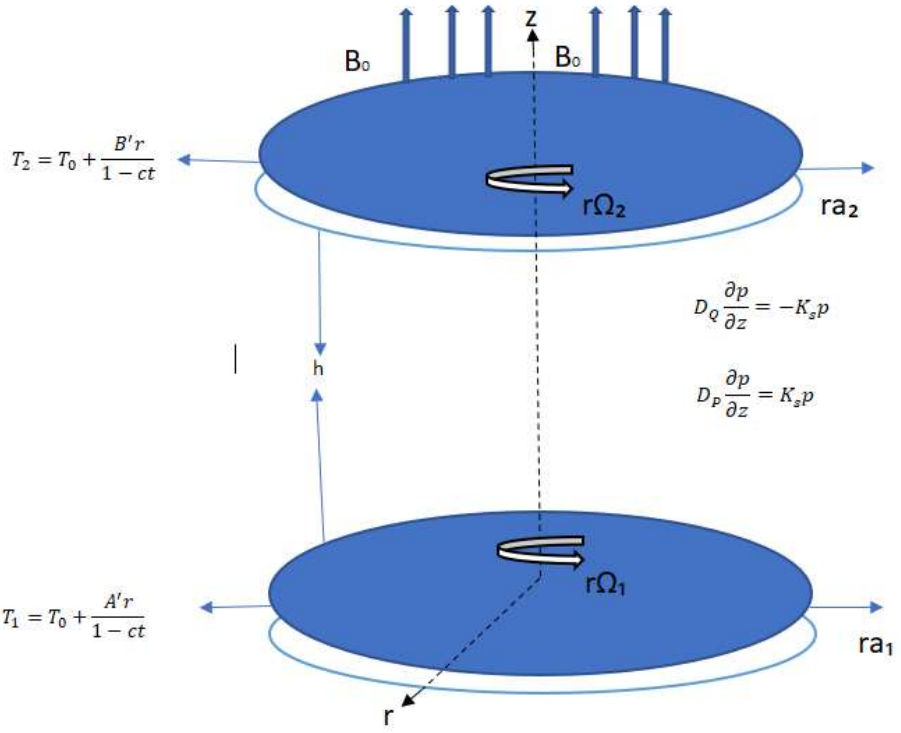

Fig. 3.1 Flow geometry

A model of the HH reaction for isothermal cubic autocatalysis with reactant and product P and Q,and given by

$$P + 2Q \rightarrow 3Q \qquad rate = K_c pq^2, \tag{3.1}$$

$$P \rightarrow Q \qquad rate = K_s P, \tag{3.2}$$

Where p,q represent the concentration of chemical species P and Q, and K_s,K_c are rate magnitudes. The momentum and continuity equation the implementation of boundary layer theory is as follows:

$$u_r + \frac{u}{r} + w_z = 0, \tag{3.3}$$

$$u_t + uu_r + wu_z - \frac{v^2}{r} = \frac{-1}{\rho_{nf}} p_r^* + \frac{u_{nf}}{\rho_{nf}} \left(u_{rr} + \frac{1}{r} u_r - \frac{u}{r^2} + u_{zz} \right) - \frac{\sigma_{nf}}{\rho_{nf}} \frac{B_o}{1+m^2} (u - mv) + \frac{\sigma_{nf} B_o^2 u}{\rho_{nf}}, \tag{3.4}$$

$$v_t + uv_r + wv_z + \frac{uv}{r} = \frac{-1}{\rho_{nf}} p_r^* + \frac{u_{nf}}{\rho_{nf}} \left(v_{rr} + \frac{1}{r} v_r - \frac{v}{r^2} + v_{zz} \right) - \frac{\sigma_{nf}}{\rho_{nf}} \frac{B_o}{1+m^2} (v + mu) + \frac{\sigma_{nf} B_o^2 v}{\rho_{nf}}, \tag{3.5}$$

$$w_t + uw_r + ww_z - \frac{v^2}{r} = \frac{-1}{\rho_{nf}} p_z^* + \frac{\mu_{nf}}{\rho_{nf}} \left(w_{rr} + \frac{1}{r} w_r + w_{zz} \right), \tag{3.6}$$

$$\begin{aligned} & T_t + uT_r + wT_z + \gamma_1 \left(\begin{array}{c} T_{tt} + u_t T_r + 2uT_{tr} + 2wT_{tz} + w_t T_z + uu_r T_r + ww_z T_z + uw_r T_r \\ + wT_r T_z + 2uwT_{tz} + u^2 w_{rr} + w^2 T_{zz} \end{array} \right) \\ = \; & \frac{K_{nf}}{(\rho C_p)_{nf}} \left(T_{rr} + \frac{1}{r} T_r + T_{zz} \right) - \frac{1}{(\rho C_p)_{nf}} \frac{\partial q_r}{\partial z}, \end{aligned} \tag{3.7}$$

$$p_t + up_r + wp_z = D_p \left(p_{rr} + \frac{1}{r} p_r + p_{zz} \right) - K_c p q^2, \tag{3.8}$$

$$q_t + uq_r + wq_z = D_Q \left(q_{rr} + \frac{1}{r} p_r + q_{zz} \right) + K_c p q^2, \tag{3.9}$$

Density, viscosity, thermal conductivity, electrical conductivity, and specific heat are all represented by $\rho, \mu, k, \sigma, C_p$. B_o is magnetic field applied in normal direction.Temperature at lower disk $T_1 = T_o + \frac{A'r}{1-ct}$, at upper disk $T_2 = T_o + \frac{B'r}{1-ct}$. T_o denotes the reference temperature, dimensional constants are A and B with dimensions KL^{-1}. n_f is a subscript, a term used

to describe the physical properties of nanofluids in addition Carbon nanotubes are reffered as CNTs. The discharge coefficient are described by D_p and D_q. Suitable boundaries are:

$$u = \frac{ra_1}{1-ct}, v = \frac{r\Omega_1}{1-ct}, w = 0, T = T_1 = T_o + \frac{A'r}{1-ct}, D_p\frac{\partial p}{\partial z} = K_s p, D_q\frac{\partial p}{\partial z} = -K_s p, \text{ at } z = 0. \tag{3.10}$$

$$u = \frac{ra_2}{1-ct}, v = \frac{r\Omega_2}{1-ct}, w = 0, T = T_2 = T_o + \frac{B'r}{1-ct}, p \to p_o \ , q \to 0 \text{ at } z = h. \tag{3.11}$$

The equation below defines the radiative heat flux.

$$\begin{aligned} q_r &= \frac{4\sigma_1^*}{3k_1^*}\frac{\partial T^4}{\partial z} \\ \frac{1}{(\rho C_p)}\frac{\partial q_r}{\partial z} &= \frac{1}{(\rho C_p)}\frac{\partial}{\partial z}\left(\frac{4\sigma_1^*}{3k_1^*}4T^3\frac{\partial T}{\partial z}\right), \end{aligned} \tag{3.12}$$

$$\begin{aligned} & T_t + uT_r + wT_z + \epsilon_1 \left(\begin{array}{c} T_{tt} + u_t T_r + 2uT_{tr} + 2wT_{tz} + w_t T_z + uu_r T_r + \\ ww_z T_z + uw_r T_r + wT_r T_z + 2uwT_{tz} + u^2 w_{rr} + w^2 T_{zz} \end{array} \right) \\ = \ & \frac{K_{nf}}{(\rho C_p)_{nf}}\left(T_{rr} + \frac{1}{r}T_r + T_{zz}\right) + \frac{16\sigma_1^*}{(\rho C_p)_{nf}3k_1^*}\left(3T^2\left(\frac{\partial T}{\partial z}\right)^2 + T^3\frac{\partial T}{\partial z^2}\right), \end{aligned} \tag{3.13}$$

The temperature in terms of thermal stratification parameter can be written as [41].

$$T = T_2\left[1 + \left(\frac{1}{\theta_w + s}\right)\theta\right], \tag{3.14}$$

where $\theta_w = \frac{T_0(1-ct)}{A'r}$ is temperature ratio parameter.

Thermo-physical traits of CNTs are:

$$A = \frac{\mu_{nf}}{\mu_f} = \frac{1}{(1-\phi)^{2.5}}, \tag{3.15}$$

$$B = \frac{\rho_{nf}}{\rho_f} = (1-\phi) + \frac{\rho_{cnt}}{\rho_f}\phi, \tag{3.16}$$

$$C = \frac{(\rho C_p)_{nf}}{(\rho C_p)_f} = (1-\phi) + \frac{(\rho C_p)_{CNT}}{(\rho C_p)_f}\phi, \tag{3.17}$$

$$D = \frac{k_{nf}}{k_f} = \frac{(1-\phi) + 2\phi\frac{k_{CNT}}{k_{CNT}-k_f}\ln\frac{k_{CNT}+k_f}{2k_f}}{(1-\phi) + 2\phi\frac{k_f}{k_{CNT}-k_f}\ln\frac{k_{CNT}+k_f}{2k_f}}, \tag{3.18}$$

$$A_2 = \frac{\sigma_{nf}}{\sigma_f} = 1 + \frac{3\phi\left(\frac{\sigma_{CNT}}{\sigma_f} - 1\right)}{\left(\frac{\sigma_{CNT}}{\sigma_f} + 2\right) - \left(\frac{\sigma_{CNT}}{\sigma_f} - 1\right)}. \tag{3.19}$$

Table 3.1 Thermophysical properties of base fluid Ethylene glycol and CNTs.

Physical Properties	Ethylene Glycol	SWCNT	MWCNT
$\rho\left(\frac{kg}{m^3}\right)$	1115	2600	1600
$c_p\left(\frac{J}{kg.K}\right)$	2430	425	796
$K\left(\frac{W}{m.K}\right)$	0.253	6600	3000
$\sigma\left(\frac{s}{m}\right)$	1.07×10^{-6}	1×10^{6}	1×10^{5}

3.1.1 Similarity tansformations

Non dimensional similarity tansformation are given as:

$$\begin{aligned} u &= \frac{r\Omega_1}{1-ct}f'(\eta), v = \frac{r\Omega_1}{1-ct}g(\eta), w = \frac{2h\Omega_1}{\sqrt{1-ct}}f(\eta), \theta = \frac{T-T_2}{T_1-T_o}, \\ p^* &= \frac{\rho\Omega_1 v}{(1-ct)^2}\left(P(\eta) + \frac{r^2}{2h^2}\epsilon\right), \eta = \frac{z}{h\sqrt{1-ct}}, p = c_o\widetilde{\phi}, q = c_o\widetilde{l}, \end{aligned} \tag{3.20}$$

Obtaining governing equations are:

$$A_1\left(f' + \frac{\eta}{2}f''\right) + \left(f'^2 - 2ff'' - g^2\right) + \frac{A}{B\,\mathrm{Re}}f''' - \epsilon - \frac{A_2}{B}\frac{M}{1+m^2}\left(f' - mg\right) - \frac{A_2 M}{B}f' = 0, \tag{3.21}$$

$$
\begin{aligned}
& A_1\left[\left(g+\frac{1}{2}\eta g'\right)A_1+2\left(f'g-g'f\right)\right] \\
= \quad & \frac{A}{B\,\mathrm{Re}}g''-\frac{A_2}{B}\frac{M}{1+m^2}\left(g+mf'\right)-\frac{A_2}{B}Mg,
\end{aligned}
\tag{3.22}
$$

$$
-\frac{1}{B\rho_f}p'^{*}=\left(A_1\left(f+\eta f'\right)-4ff'\right)+\frac{A}{B\,\mathrm{Re}}f'',
\tag{3.23}
$$

$$
\begin{aligned}
& A_1\left(s+\theta+\frac{1}{2}\eta\theta'\right)+f'\left(s+\theta+\frac{1}{2}\eta\theta'\right)-2f\theta' \\
& +\gamma\begin{bmatrix}
A_1\left(2\left(s+\theta+\frac{1}{2}\eta\theta'\right)+\frac{1}{4}\left(3\eta\theta'+\eta^2\theta''\right)\right) \\
+\left(f'+\frac{1}{2}\eta f''\right)(s+\theta)+2\left(s+\theta+\frac{1}{2}\eta\theta'\right) \\
-4f\left(\frac{3}{2}\theta'+\frac{\eta}{2}\theta''\right)+\left(f'+\eta f''\right)\theta'+\frac{1}{A_1}f'^2(s+\theta) \\
-\frac{4}{A_1}f'^2\theta'-\frac{2}{A}ff''(s+\theta)-\left(\frac{4}{A_1}ff'\theta'+\frac{4}{A_1}f^2\theta''\right) \\
+\frac{2}{A_1}\left(s+\theta+\frac{1}{2}\eta\theta'\right)+\frac{4}{A_1}f\left(\frac{1}{2}\eta\theta''+\frac{3}{2}\theta'\right)
\end{bmatrix} \\
= \quad & \frac{1}{\mathrm{Pr}\,\mathrm{Re}\,C}\begin{bmatrix}
D\left(\theta''+(s+\theta)\right)+Rd\left(1+\frac{1}{\theta_w+s}\theta\right)^2\frac{\theta'^2}{(\theta_w+s)^2} \\
+\left(1+\frac{1}{\theta_w+s}\theta\right)^3\frac{\theta''}{(\theta_w+s)}
\end{bmatrix},
\end{aligned}
\tag{3.24}
$$

$$
\frac{1}{2}\eta\widetilde{\phi'}-\frac{2}{A_1}f\widetilde{\phi'}-\frac{1}{Sc}\widetilde{\phi''}+k1\widetilde{\phi}l^2=0,
\tag{3.25}
$$

$$
\frac{1}{2}\eta\widetilde{l'}-\frac{2}{A_1}f\widetilde{l'}-\frac{1}{Sc}\widetilde{l''}+k1\widetilde{\phi}l^2=0.
\tag{3.26}
$$

The following are the boundary conditions:

$$
\begin{aligned}
f(0) &= 0,\ f(1)=0,\quad f'(0)=\gamma_1,\ f'(1)=\gamma_2, g(0)=1, \\
g(1) &= \Omega, \theta(0)=1-s, \theta(1)=0, P(0)=0,
\end{aligned}
\tag{3.27}
$$

M denotes the saturation magnetization parameter.The unsteadiness parameter is A_1, Scale stretching parameters γ_1 and γ_2 are referred to as lower and upper disks, respectively. Schmidt's

number is Sc. Pr is the Prandtl number. Ω is the rotation parameter.K_1, K_2 are the homogeneous and heterogeneous response strength measures, respectively. m represents hall current.The ratio of diffusivity is δ. γ is the thermal relaxation time. R_d, s are used to symbolise the parameter of thermal radiation and the parameter of thermal stratification respectively.

Here

$$\begin{aligned} M &= \frac{\sigma_f B_o^2 (1-ct)}{\rho_f (1+m^2)}, A_1 = \frac{c}{\Omega_1}, \gamma_1 = \frac{a_1}{\Omega_1}, \gamma_2 = \frac{a_2}{\Omega_2}, Sc = \frac{h^2 c}{D_p}, \Pr = \frac{\nu_f (\rho C_P)_f}{k_f} \\ \Omega &= \frac{\Omega_2}{\Omega_1}, k1 = \frac{K_c c_o^2 (1-ct)}{c}, k2 = \frac{K_s h (1-ct)^{1/2}}{D_P}, \delta = \frac{D_Q}{D_P}, \gamma = \frac{c\epsilon 1}{1-ct}, \\ Rd &= \frac{-16\sigma^* T_2^3}{3k_f k^*}, s = \frac{B'}{A'}, \end{aligned} \tag{3.28}$$

Considering the chemical species are the same resulted in the hypothesis $\delta = 1$, and ultimately $\widetilde{l}(\eta) + \widetilde{\phi}(\eta) = 1$ was chosen.

The equations (3.25 and 3.26) are simplified as a result of this hypothesis.

$$\frac{1}{Sc}\widetilde{\phi''} - \frac{1}{2}\eta\widetilde{\phi'} - \frac{2}{A_1} f\widetilde{\phi'} - k1\left(1-\widetilde{\phi}\right)^2 \widetilde{\phi} = 0, \tag{3.29}$$

$$\widetilde{\phi'}(0) = K_2\widetilde{\phi'}(0), \widetilde{\phi'}(1) \to 1, \tag{3.30}$$

By differentiating equation (3.21) we get the following equation:

$$\begin{aligned} & A_1\left(\frac{3}{2}f'' + \frac{\eta}{2}f'''\right) - \left(2ff''' + 2gg'\right) \\ = \; & \frac{A}{B\,\mathrm{Re}} f^{iv} - \frac{A_2}{B}\frac{M}{1+m^2}\left(f'' - mg'\right) - \frac{A_2 M}{B} f'', \end{aligned} \tag{3.31}$$

3.2 Surface drag force coefficient and rate of heat transfer

Shear stress in the radial and tangential directions τ_{zr} and $\tau_{z\theta}$ at lower disk are:

$$\begin{aligned}\tau_{zr} &= \mu_{nf} u_z|_{z=0} = \frac{\mu_f r\Omega_1 f''(0)}{h(1-\phi)^{2.5}},\\ \tau_{z\theta} &= \mu_{nf} u_z|_{z=0} = \frac{\mu_f r\Omega_1 g'(0)}{h(1-\phi)^{2.5}}.\end{aligned} \tag{3.32}$$

The combined shear stress is given by:

$$\tau_w = \left(\tau_{zr^2} + \tau_{z\theta^2}\right)^{1/2}, \tag{3.33}$$

The components of surface drag force coefficients at lower and upper disks are:

$$C_{f_1} = \frac{\tau_w|_{z=0}}{\rho_f (r\Omega_1)^2} = \frac{1}{\mathrm{Re}\,(1-\phi)^{2.5}}\left[\left(f''(0)\right)^2 + \left(g'(0)\right)^2\right]^{1/2}, \tag{3.34}$$

$$C_{f_2} = \frac{\tau_w|_{z=h}}{\rho_f (r\Omega_2)} = \frac{1}{\mathrm{Re}\,(1-\phi)^{2.5}}\left[\left(f''(1)\right)^2 + \left(g'(1)\right)^2\right]^{1/2}, \tag{3.35}$$

here, the Reynolds number is *Re*.

Heat transfer rate for both disks are:

$$\begin{aligned}N_{u_{x1}} &= \frac{hq_w}{k_f (T_1 - T_0)}|_{z=0}.\\ N_{u_{x1}} &= \frac{hq_w}{k_f (T_1 - T_0)}|_{z=h}.\end{aligned} \tag{3.36}$$

Where q_w is the wall heat flux heat flux.

$$\begin{aligned}q_w|_{z=0} &= -k_{hnf}\frac{\partial T}{\partial z}|_{z=0} + \frac{16\sigma_1^* T_1^3}{3k_1^*}\frac{\partial T}{\partial z}|_{z=0}\\ q_w|_{z=h} &= -k_{hnf}\frac{\partial T}{\partial z}|_{z=h} + \frac{16\sigma_1^* T_1^3}{3k_1^*}\frac{\partial T}{\partial z}|_{z=h}\end{aligned} \tag{3.37}$$

Non-dimensional heat transfer rate are:

$$\begin{aligned}(1-ct)^{1/2}\,Nu_1 &= -\left(\frac{k_{hnf}}{k_f}+\left(Rd\,(1+(\theta_w-1)\,\theta\,(0))^3\right)\right)\theta'\,(0)\,.\\ (1-ct)^{1/2}\,Nu_2 &= -\left(\frac{k_{hnf}}{k_f}+\left(Rd\,(1+(\theta_w-1)\,\theta\,(1))^3\right)\right)\theta'\,(1)\,. \qquad (3.38)\end{aligned}$$

3.3 Results and discussions

This section portrays the axial velocity $f\ (\eta)$, radial velocity $f\,'(\eta)$ and thermal profile $\theta\,(\eta)$, concentration field $\Phi\,(\eta)$, drag coefficient, and heat transfer rate for various values of the relevant parameters in graphical and tabular style. Flow parameters are saturation magnetization parameter M, unsteadiness parameter A_1,Scale stretching parameters γ_1&γ_2, Schmidt's number Sc, Prandtl number Pr, Ω rotation parameter, the homogeneous reaction parameter K_1 and the heterogeneous reaction parameter K_2,The ratio of diffusivity parameter δ, thermal relaxation time parameter γ, thermal radiation parameter R_d, thermal stratification parameter s, volume fraction coefficient Φ and Reynolds number Re .we set the parameters with ranges to attain the desired results: $0 \leq M \leq 2.1, 0.0 \leq A_1 \leq 2.4, 0.0 \leq \gamma_1 \leq 0.4, 0.0 \leq \gamma_2 \leq 2.7, 0.0 \leq \gamma \leq 1, 0.0 \leq \Omega \leq 2, 6.4 \leq \mathrm{Pr} \leq 6.9, 0.0 \leq m \leq 2.4, 0.03 \leq 0.06, 0.0 \leq 2.6, 0.0 \leq 0.3, 0.2 \leq R_d \leq 0.6$. Here, $SWCNTs$ are represented by sloid lines (——) and$MWCNTs$ are given by dashed line(- - - -).

Figs. 3.2 -3.3 are sketched for Axial velocity $f\ (\eta)$ and Radial velocity $f\,'(\eta)$ profiles on Re (Reynolds number) for the single-wall ($SWCNTs$) and multi-wall carbon nanotubes ($MWCNTs$). For both types of nanotubes, increasing values of Re will alter the both axial velocity and Radial velocity profiles. As Re increases, inertial forces take over, resulting in a decrease in velocity profiles. The effect of the lower disk stretching parameter γ_1 on the radial and axial velocity profiles is shown in Figs. 3.4 and 3.5. The magnitude of radial velocity increases near the lower disk, while the converse occurs towards the top disk. The axial velocity, on the other hand, increases throughout the system. Because stretching in the lower disk is rising, radial and axial velocity profiles near the upper disk take on negative values. The effect of stretching rate parameter γ_2 on Axial and Radial velocities at upper and lower disks is shown in Figs. 3.6 and 3.7. At near the lower disk axial $f\ (\eta)$and radial $f\,'(\eta)$ velocities decreases

in the entire system. But at near the upper disk radial velocity $f'(\eta)$ behaves oppositvely, it shows that disk's increased stretching rate at $z = h$. To see how ϕ effects on $f(\eta)$ and $f'(\eta)$ Figs. 3.8 and 3.9 are sketched, It's worth noting that the radial velocity profile is growing as the value of ϕ rises. The axial velocity increases at the lower disc and after reflection, but drops as the nanoparticle volume percentage increases.

Fig.3 .10 displays the Reynolds number Re behaviour on the tangential velocity profile $g(\eta)$. The tangential velocity decreases as the value of Re increases. The inertial forces rise as Re is increased. To visualize the impact of magnetic field parameter on Tangential velocity Fig. 3.11. is sketched, it shows that as we increase the value of M velocity profile decreases.The physical reason for this decrease in velocity profile is because raising the magnetic field parameter creates the retarding force, which slows down particle motion.Fig. 3.12. shows how the velocity profile $g(\eta)$ changes as the volume percentage of nanoparticles ϕ grows. The velocity profile increases as we increase the ratio of nanoparticles, this due to the addition of solid nanoparticles causes the boundary layer to thin. Fig. 3.13 shows the impact of stretching parameter γ_2, for high values of stretching parameter the tangential velocity profile $g(\eta)$ increases. The stretching rate increases for bigger values of γ_2 and hence the velocity increases. For the idea effect of Ω on tangential velocity, Fig. 3.14 is sketched. Velocity increases as value of rotation parameter increases.

In Fig. 3.15 both single-wall ($SWCNTs$) and multi-wall($MWCNTs$) carbon nanotubes exhibit a thermal profile $\theta(\eta)$ for the thermal relaxation parameter γ. The higher the rate of thermal relaxation, the higher the thermal profile. This is due to the thickness of the thermal boundary layer thins as the value of the thermal relaxation parameter increases. When the quantity of nanoparticles ϕ is increased, the heat transmission rate reduces. Decline in thermal profile for multi-wall and single-wall nanoparticles has shown in Fig. 3.16. Decline in the thermal profile $\theta(\eta)$ is caused by an increase in the unsteadiness parameter A_1,drawn for both type of nanoparticles in Fig. 3.17. Influence of radiation parameter Rd on $\theta(\eta)$ is portrayed in Fig.3.18. Here the fluid temperature increases for larger Rd. In fact when we increase radiation parameter, the mean absorption coefficient decreases which enhances the rate of radiative heat transfer to the fluid. Fig.3.19 presents the behavior of temperature profile $\theta(\eta)$ for thermal stratification parameter S. Temperature profile and thermal boundary layer

thickness are decrease via S. Actually the temperature difference between two disks decreases gradually which shows reduction in fluid temperature. Here ($MWCNTs$) are found to be more dominant than other types of carbon nanotubes, ($SWCNTs$).

Figs. 3.20-3.22 are plotted for both ($SWCNTs$) and ($MWCNTs$) to discuss concentration field $\psi(\eta)$ versus k1, k2 and Sc. Fig. 3.20 shows that concentration field decreases for higher values of homogeneous reaction parameter k1.The same behaviour observed in Fig. 3.21 for heterogeneous reaction parameter k2. This is due to the fact that concentration decreases over time as reactants are consumed in HH reactions. In Fig. 3.22, the effect of Schmidt number is represented. Decreasing trend is observed for increasing the value of Sc. As Sc is the ratio of momentum to mass diffusivity, greater Sc indicates the smaller mass diffusivity which results in the reduction in fluid concentration $\psi(\eta)$.

Table 3.2 and 3.3 demonstrates how the drag force increases as the Hall current parameter is increased. As M increases, the frictional forces rise, increasing the barrier to fluid motion and the coefficient of drag force. Increasing Re generates a rise in inertial forces, which leads to an increase in drag coefficient. Also shows the drag force coefficients for stretching parameters γ_1 and γ_2 at $z = 0$ and $z = h$. Table. 3. 2 is for single-wall nanoparticles, Table 3.3 for multi-wall nanoparticles.

The temperature profile for both disks is reduced as the thermal stratification parameter s is increased, as seen in Table 3.4 and 3.5 . The rate of heat transfer is reduced by increasing Pr for single and multiwall carbon nanotubes at lower disc due to a decrease in thermal boundary layer thickness. For both types of barriers, it is rising at the upper disk. The rate of heat transfer for both the disk and both walls increases as the radiation parameter R_d is increased.

Table 3.4 is for single-wall nanoparticles, Table 3.5 for multi-wall nanoparticles.

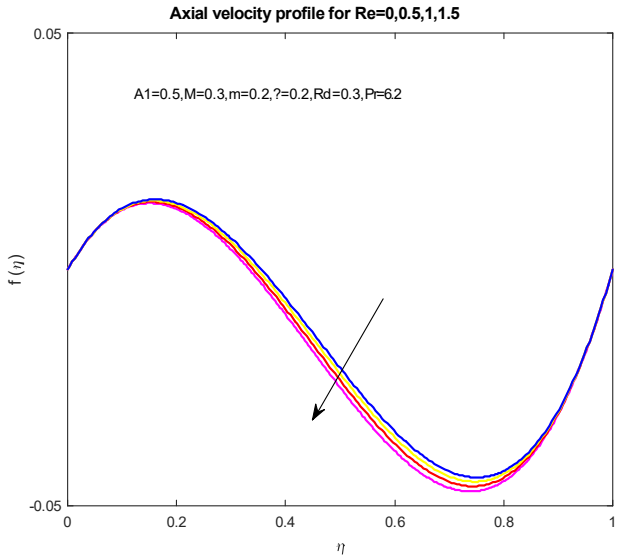

Fig.3.2 Change in $f(\eta)$ vs.Re

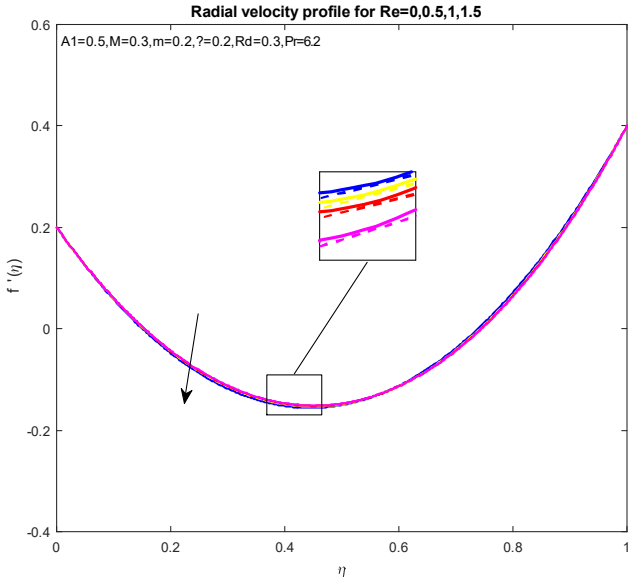

Fig.3.3 Change in $f'(\eta)$ vs.Re

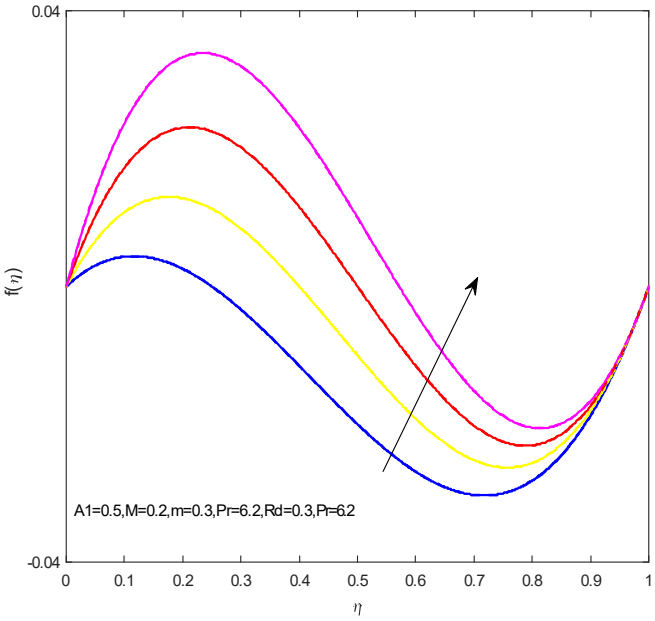

Fig.3.4 Change in $f(\eta)$ vs.γ_1

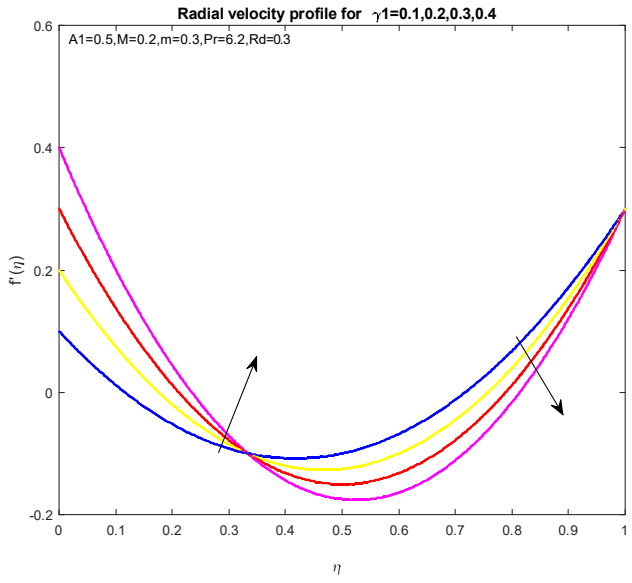

Fig.3.5 Change in $f'(\eta)$ vs.γ_1

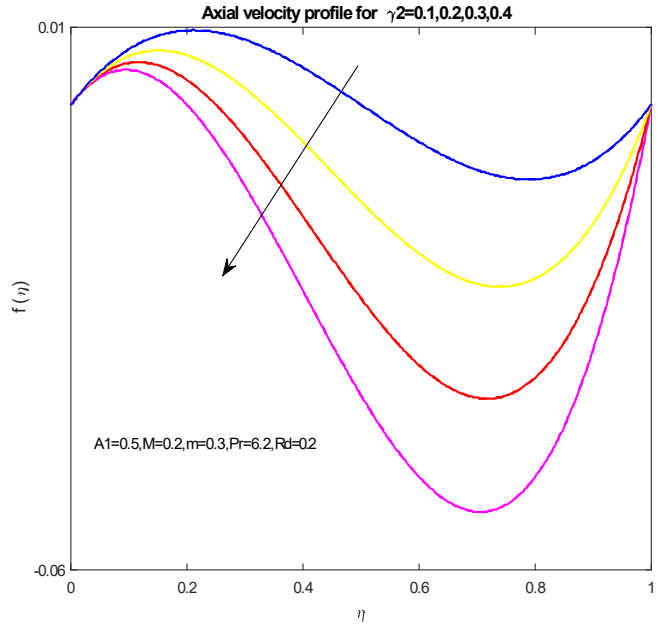

Fig.3.6 Change in $f(\eta)$ vs.γ_2

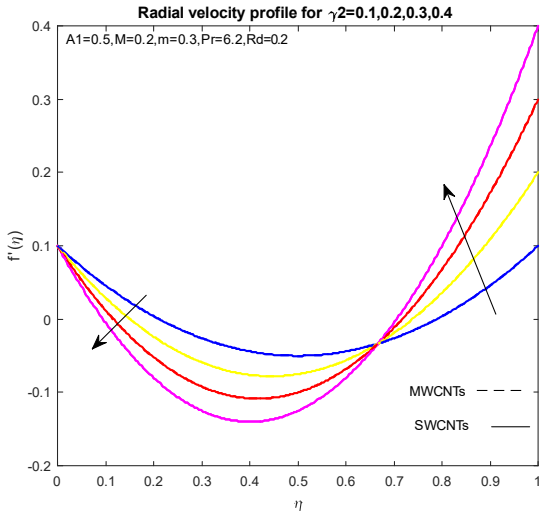

Fig.3.7 Change in $f'(\eta)$ vs.γ_2

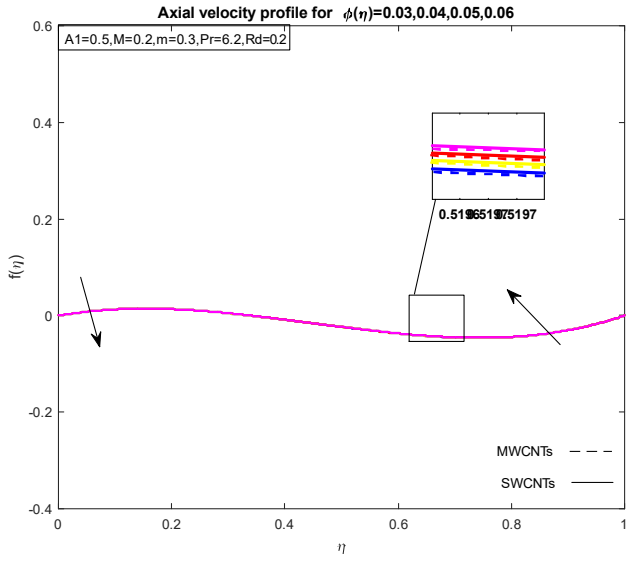

Fig.3.8 Change in $f\ (\eta)$ vs.ϕ

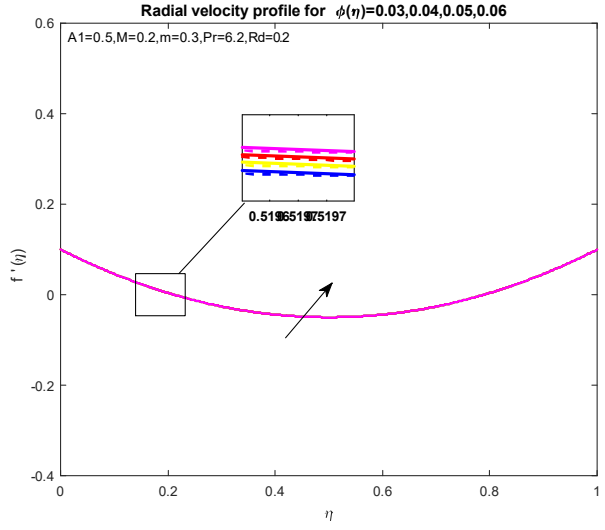

Fig.3.9 Change in $f'\,(\eta)$ vs.ϕ

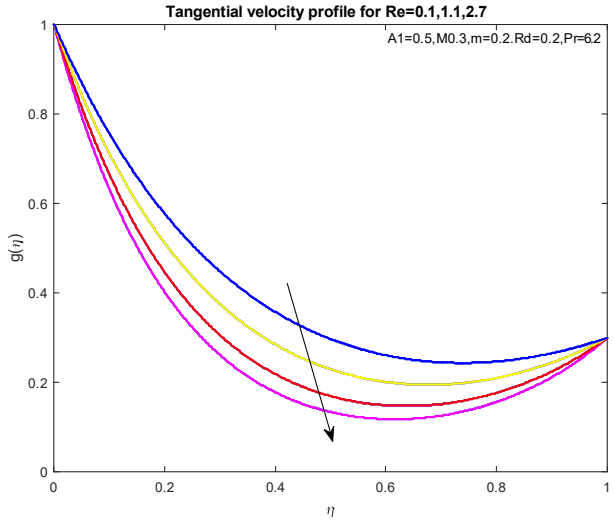

Fig.3.10 Change in $g(\eta)$ vs.Re

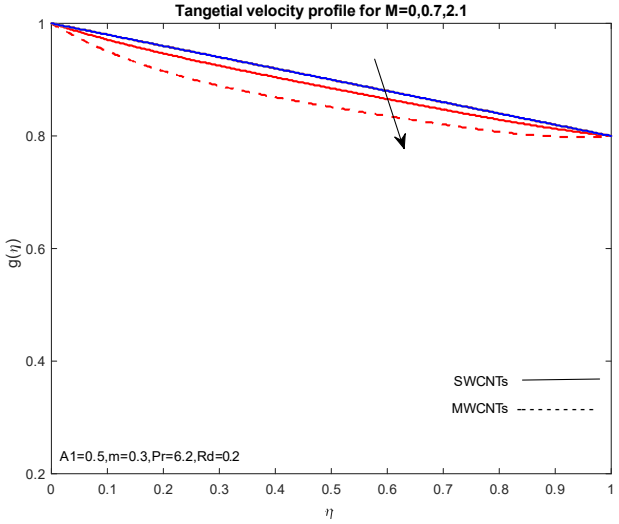

Fig.3.11 Change in $g(\eta)$ vs.M

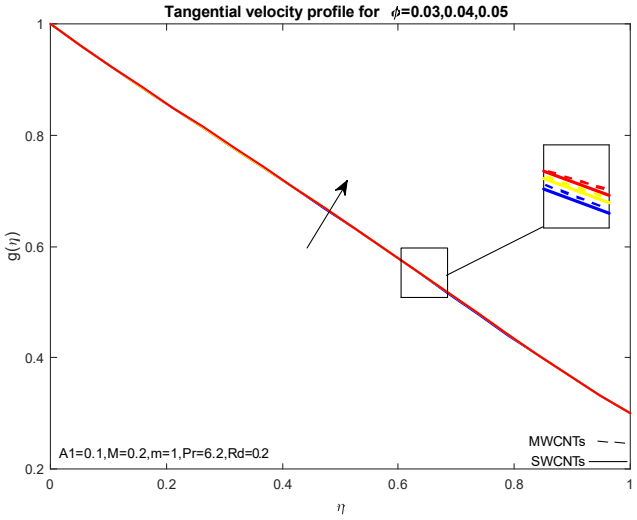

Fig.3.12 Change in $g(\eta)$ vs.ϕ

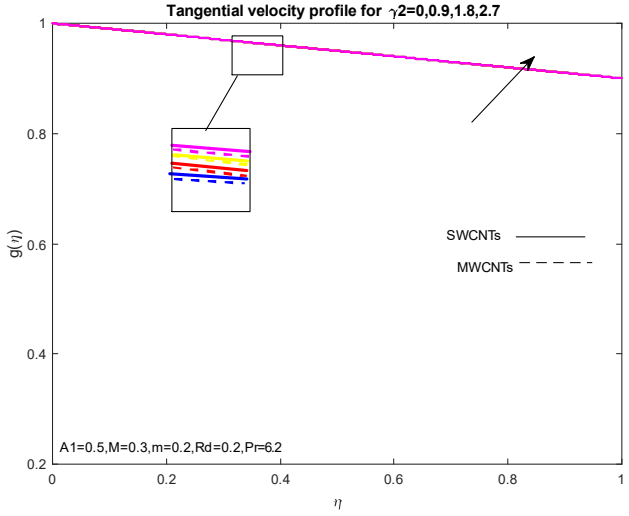

Fig.3.13 Change in $g(\eta)$ vs.γ_2

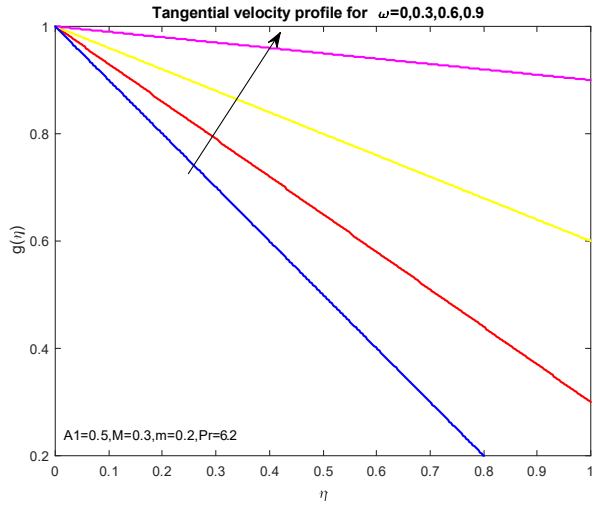

Fig.3.14 Change in $g(\eta)$ vs.Ω

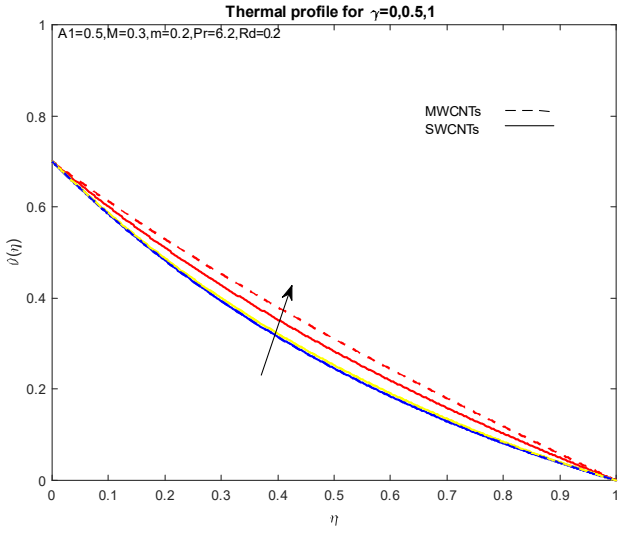

Fig.3.15 Change in $\theta(\eta)$ vs.γ

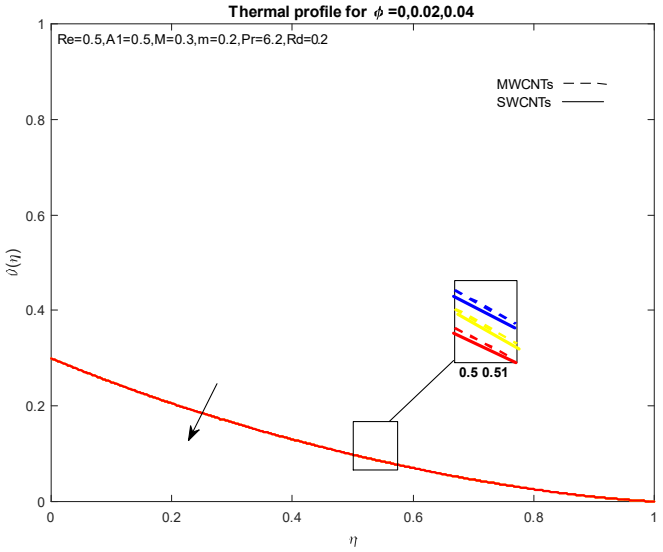

Fig.3.16 Change in $\theta(\eta)$ vs.ϕ

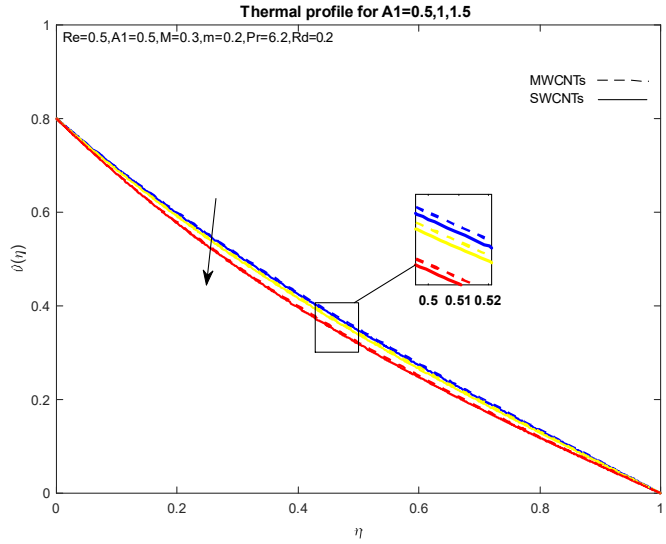

Fig.3.17 Change in $\theta(\eta)$ vs.A_1

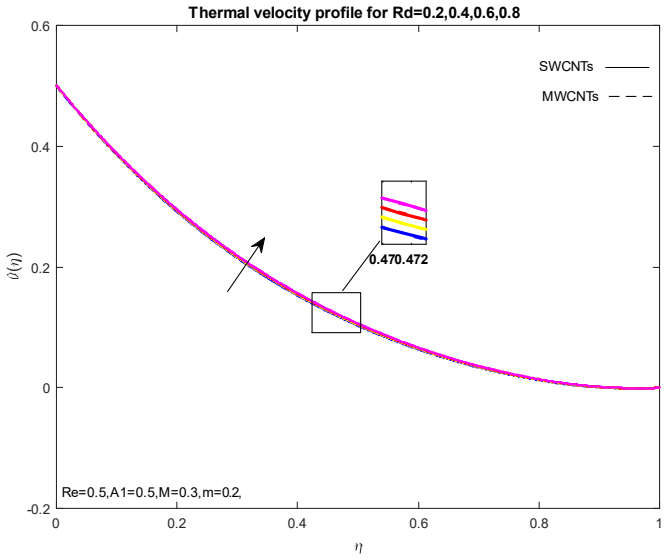

Fig.3.18 Change in $\theta(\eta)$ vs.Rd

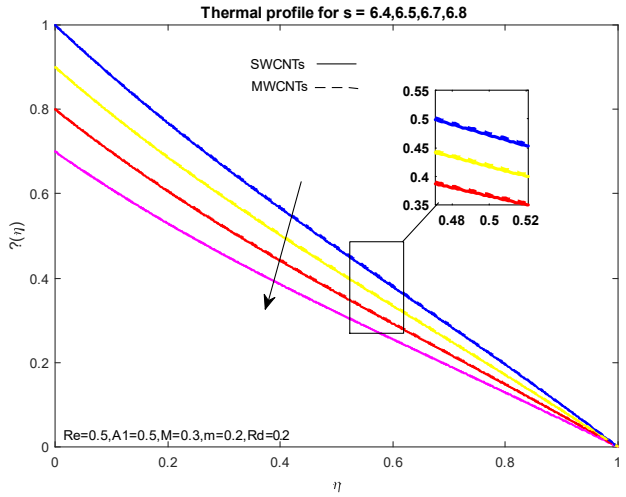

Fig.3.19 Change in $\theta(\eta)$ vs.s

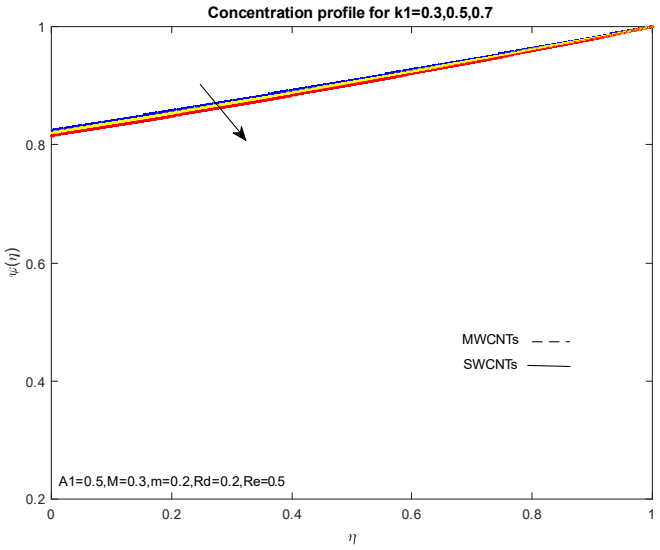

Fig.3.20 Change in $\psi(\eta)$ vs.K_1

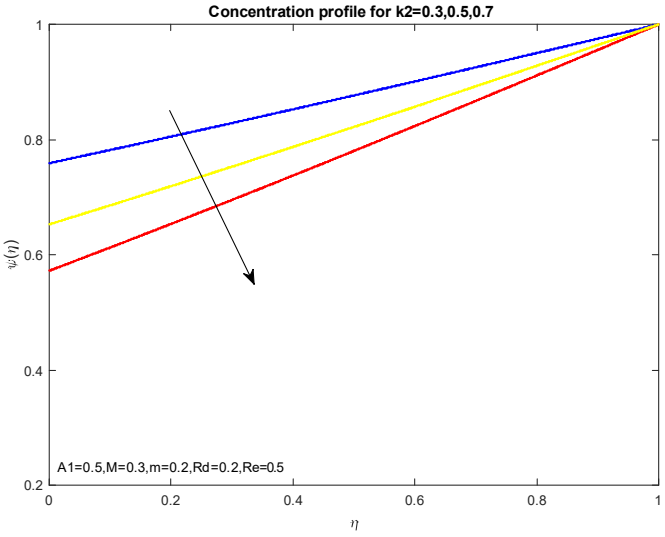

Fig.3.21 Change in $\psi(\eta)$ vs.K_2

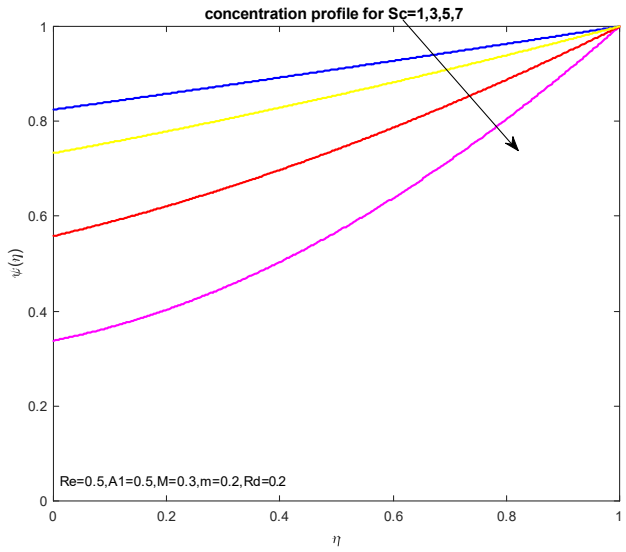

Fig.3.22 Change in $\psi(\eta)$ vs.Sc

Table 3.2 Numerical values of Skin friction coefficient for SWCNT

$A_1 = 0.5, \mathrm{Pr} = 6.7, \Omega = 0.5, s = 0.4, k1 = 0.1, k2 = 0.1, Sc = 1$

m	M	Re	γ_1	γ_2	SWCNTs(C_1)	SWCNTs(C_2)
0	0				1.02009	1.19338
	0.5				1.06637	1.16579
0.5	0				1.02009	1.19338
	0.5				1.08068	1.15901
	1				1.14339	1.16934
1	0.5	0.5			1.08068	1.15901
		1			1.09870	1.17917
		1.5			1.16080	1.9933
			0.1		1.08068	1.15901
			0.2		1.43290	1.36137
			0.1	0.2	1.08068	1.15901
				0.4	1.40102	2.00825

Table 3.3 Numerical values of Skin friction coefficient for MWCNT

$A_1 = 0.5, \mathrm{Pr} = 6.7, \Omega = 0.5, s = 0.4, k1 = 0.1, k2 = 0.1, Sc = 1$

m	M	Re	γ_1	γ_2	MWCNTs (C_1)	MWCNTs(C_2)
0	0				1.0247	1.19405
	0.5				1.06687	1.16951
0.5	0				1.02476	1.19405
	0.5				1.07952	1.26354
	1				1.13593	1.27605
1	0.5	0.5			1.07952	1.16354
		1			1.08981	1.18353
		1.5			1.10667	1.20367
			0.1		1.07952	1.16354
			0.2		1.43181	1.36611
			0.1	0.2	1.07952	1.16354
				0.4	1.39573	2.01537

Table 3.4 Numerical values of Heat transfer rate for SWCNTs when.

$A_1 = 0.5, \mathrm{Pr} = 6.7, \Omega = 0.5, s = 0.4, k1 = 0.1, k2 = 0.1, Sc = 1$

S	Pr	R_d	SWNTs$\left(-\frac{k_{nf}}{k_f}\theta'(0)\right)$	SWCNTs$\left(-\frac{k_{nf}}{k_f}\theta'(1)\right)$
0.2			1.01732	1.22531
0.4			0.786383	0.906309
0.6			0.586036	0.54263
0.2	6.7		1.017321	1.22531
	6.8		1.01726	1.21542
	6.9		1.01679	1.20563
		0.5	1.01732	1.22531
		0.6	1.998331	1.25062
		0.7	1.99983	1.27661

Table 3.5 Numerical values of Heat transfer rate for MWCNTs when.

$A_1 = 0.5, \mathrm{Pr} = 6.7, \Omega = 0.5, s = 0.4, k1 = 0.1, k2 = 0.1, Sc = 1$

S	Pr	R_d	MWCNTs$\left(-\frac{k_{nf}}{k_f}\theta'(0)\right)$	MWCNTs$-\frac{k_{nf}}{k_f}\theta'(1)$
0.2			0.992042	1.19958
0.4			0.768216	0.886326
0.6			0.575242	0.527718
0.2	6.7		0.992042	1.19958
	6.8		0.992282	1.19969
	6.9		0.992521	1.19970
		0.5	0.992042	1.9958
		0.6	0.993116	1.22497
		0.7	0.998607	1.25106

Chapter 4

Hybrid nanofluid squeezing flow with Hall current and non-uniform source/sink

In this chapter, we investigated hybrid nanofluid squeezing flow based engine oil as the base fluid, suspended in the midst of two revolving extensible discs with copper and gold as nano-particles, with Hall current.The intended model is enhanced under the effect of cattaneo-christov(C-C) heat flux and thermal stratification.The influenced of nonlinear thermal radiation is demonstrated in the unique nature of the problem.Using adequate similarity transformations, a set of partial differential equations are converted into ordinary differential equations. The bvp4c built-in function of the MATLAB method is used to address the obtained system of equations. The results of emerging parameters are portrayed visually for axial,radial and tangential velocities and temperature.It is noted that for hall current shows opposite behavior for radial and tangential velocities

4.1 Mathematical modelling

We consider time-dependent squeezing flow based engine oil and containing copper(Cu) and gold(Ag) as nano-particles. A thermal segregated medium is used to separate heat transfer from the base fluid and the field current effect. The flow is known between two parallel discs

of length h. The discs are stretched at $a_1$and a_2, respectively, along angular velocities of Ω_1 and Ω_2 about their axis. $V[u(r,\theta), v(r,\theta), w(r,\theta)]$ is represented the steady state velocity, with (u, v, w) as velocity componentswith respect to(r, θ, z) directions. T_1 and T_2 are the lower and upper disk tenperatures, respectively.

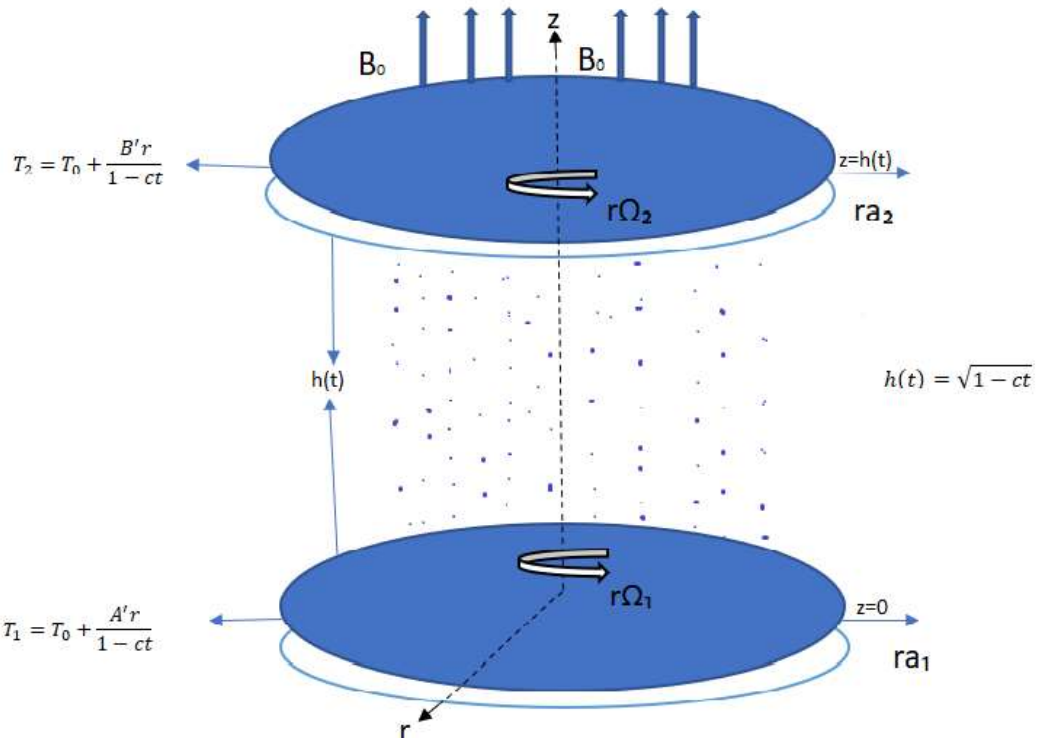

Fig. 4.1 Flow geometry

4.1.1 Governing Equations

$$u_r + \frac{u}{r} + w_z = 0. \tag{4.1}$$

$$\begin{aligned} u_r + uu_r + wu_z - \frac{v^2}{r} &= \frac{-1}{\rho_{hnf}} p_r^* + \frac{u_{hnf}}{\rho_{hnf}} \left(u_{rr} + \frac{1}{r} u_r - \frac{u}{r^2} + u_{zz} \right), \\ &\quad - \frac{\sigma_{hnf}}{\rho_{hnf}} \frac{B_o}{1+m^2} (u - mv) + \frac{\sigma_{hnf} B_o^2 u}{\rho_{hnf}}. \end{aligned} \tag{4.2}$$

$$v_r + uv_r + wv_z + \frac{uv}{r} = \frac{-1}{\rho_{hnf}} p_r^* + \frac{u_{hnf}}{\rho_{hnf}} \left(v_{rr} + \frac{1}{r} v_r - \frac{v}{r^2} + v_{zz} \right), \\ -\frac{\sigma_{hnf}}{\rho_{hnf}} \frac{B_o}{1+m^2} (v + mu) + \frac{\sigma_{hnf} B_o^2 v}{\rho_{hnf}}. \tag{4.3}$$

$$w_t + uw_r + ww_z - \frac{v^2}{r} = \frac{-1}{\rho_{hnf}} p_z^* + \frac{\mu_{hnf}}{\rho_{hnf}} \left(w_{rr} + \frac{1}{r} w_r + w_{zz} \right). \tag{4.4}$$

$$T_t + uT_r + wT_z + \gamma_1 \left(\begin{array}{c} T_u + u_t T_r + 2uT_{tr} + 2wT_{tz} + w_t T_z + uu_r T_r + ww_z T_z \\ +uw_r T_r + wT_r T_z + 2uwT_{tz} + u^2 w_{rr} + w^2 T_{zz} \end{array} \right), \\ = \frac{K_{hnf}}{(\rho C_p)_{hnf}} \left(T_{rr} + \frac{1}{r} T_r + T_{zz} \right) - \frac{1}{(\rho C_p)_{hnf}} \frac{\partial q_r}{\partial z} + \frac{Q^n}{(\rho C_p)_{hnf}}. \tag{4.5}$$

Density, viscosity, thermal conductivity, electrical conductivity, and specific heat are all represented by $\rho, \mu, k, \sigma, C_p$.$B_o$ is magnetic field applied in normal direction.Temperature at lower disk $T_1 = T_o + \frac{A'r}{1-ct}$, at upper disk $T_2 = T_o + \frac{B'r}{1-ct}$.$T_o$ denotes the reference temperature, dimensional constants are A and B with dimensions KL^{-1}. hn_f is a subscript,a term used to describe the physical properties of hybrid nanofluids. Suitable boundaries for the system are:

$$u = \frac{ra_1}{1-ct}, v = \frac{r\Omega_1}{1-ct}, w = 0, T = T_1 = T_o + \frac{A'r}{1-ct}, \quad at \quad z = 0 \tag{4.6}$$

$$u = \frac{ra_2}{1-ct}, v = \frac{r\Omega_2}{1-ct}, w = 0, T = T_2 = T_o + \frac{B'r}{1-ct}, \quad at \quad z = h \tag{4.7}$$

The equation below defines the radiative heat flux.

$$q_r = \frac{4\sigma_1^*}{3k_1^*} \frac{\partial T^4}{\partial z} \quad . \tag{4.8}$$

$$\frac{1}{(\rho C_p)} \frac{\partial q_r}{\partial z} = \frac{1}{(\rho C_p)} \frac{\partial}{\partial z} \left(\frac{4\sigma_1^*}{3k_1^*} 4T^3 \frac{\partial T}{\partial z} \right). \tag{4.9}$$

$$T_t + uT_r + wT_z + \epsilon_1 \left(\begin{array}{c} T_{tt} + u_t T_r + 2uT_{tr} + 2wT_{tz} + w_t T_z + uu_r T_r + ww_z T_z \\ +uw_r T_r + wT_r T_z + 2uwT_{tz} + u^2 w_{rr} + w^2 T_{zz} \end{array} \right),$$

$$= \frac{K_{hnf}}{(\rho C_p)_{hnf}} \left(T_{rr} + \frac{1}{r} T_r + T_{zz} \right) + \frac{16\sigma_1^*}{(\rho C_p)_{hnf} 3k_1^*} \left(3T^2 \left(\frac{\partial T}{\partial z} \right)^2 + T^3 \frac{\partial T}{\partial z^2} \right) + \frac{Q^n}{(\rho C_p)_{hnf}} \quad (4.10)$$

The temperature in terms of thermal stratification parameter can be written as:

$$T = T_2 \left[1 + \left(\frac{1}{\theta_w + s} \right) \theta \right]. \quad (4.11)$$

Where $\theta_w = \frac{T_{0(1-ct)}}{A'r}$ is temperature ratio parameter.

The non-uniform heat generation/abortion parameter Q^n is given below :

$$Q^n = \left[\frac{k_{hnf}(ra_1)}{\upsilon_{hnf}(r)} \left\{ A3(T_1 - T_0)f' + B_3 (T - T_2) \right\} \right]. \quad (4.12)$$

Thermo-physical traits of nanoparticles are:

$$A^* = \frac{\mu_{hnf}}{\mu_f} = \frac{1}{(1-\phi_1)^{2.5} (1-\phi_2)^{2.5}}. \quad (4.13)$$

$$B^* = \frac{\rho_{hnf}}{\rho_f} = (1-\phi_2) \left[(1-\phi_1) + \frac{\phi_1 \rho_{s1}}{\rho_f} \right] + \frac{\phi_2 \rho_{s2}}{\rho_f}.$$

$$C^* = \frac{(\rho C_p)_{hnf}}{(\rho C_p)_f} = (1-\phi_2) \left[(1-\phi_1) + \phi_1 \frac{(\rho C_p)_{s1}}{(\rho C_p)_f} \right] + \phi_2 \frac{(\rho C_p)_{s2}}{(\rho C_p)_f}. \quad (4.14)$$

$$D^* = \frac{k_{hnf}}{k_{bf}} = \left[\frac{k_{s2} + 2k_{bf} - 2\phi_2 (k_{bf} - k_{s2})}{k_{s2} + 2k_{bf} + \phi_2 (k_{bf} - k_{s2})} \right], \quad (4.15)$$

Where

$$\frac{k_{bf}}{k_f} = \left[\frac{k_{s1} + 2k_f - 2\phi_1 (k_f - k_{s1})}{k_{s1} + 2k_f + \phi_1 (k_f - k_{s1})} \right].$$

$$A_2^* = \frac{\sigma_{hnf}}{\sigma_f} = \left[\frac{\sigma_{s2} + 2\sigma_{bf} - 2\phi_2 (\sigma_{bf} - \sigma_{s2})}{\sigma_{s2} + 2\sigma_{bf} + \phi_2 (\sigma_{bf} - \sigma_{s2})} \right], \quad (4.16)$$

Where

$$\frac{\sigma_{bf}}{\sigma_f} = \left[\frac{\sigma_{s1} + 2\sigma_f - 2\phi_1 (\sigma_{bf} - \sigma_{s2})}{\sigma_{s1} + 2\sigma_f + \phi_1 (\sigma_{bf} - \sigma_{s2})} \right].$$

Table 4.1 Thermophysical properties of Engine oil,Copper (Cu) and Gold (Au) are:

Physical Properties	Engine oil	Cu	Au
$\sigma\left(\frac{s}{m}\right)$	55×10^{-6}	59.6×10^{6}	4.10×10^{7}
$\rho\left(\frac{kg}{m^3}\right)$	863	8933	19282
$c_p\left(\frac{J}{kg.K}\right)$	2048	385	129
$K\left(\frac{W}{m.K}\right)$	0.1404	400	310

Similarity tansformations

Non dimensional similarity tansformation are given as:

$$\begin{aligned} u &= \frac{r\Omega_1}{1-ct}f'(\eta), v = \frac{r\Omega_1}{1-ct}g(\eta), w = \frac{2h\Omega_1}{\sqrt{1-ct}}f(\eta), \theta = \frac{T-T_2}{T_1-T_o}, \\ p^* &= \frac{\rho\Omega_1 v}{(1-ct)^2}\left(P(\eta)+\frac{r^2}{2h^2}\epsilon\right), \eta = \frac{z}{h\sqrt{1-ct}}. \end{aligned} \tag{4.17}$$

Obtaining governing equations are:

$$A^* f^{iv} - B^*\left[3Sqf'' + Sq\eta f''' - 2\,\mathrm{Re}\, ff''' - 2\,\mathrm{Re}\, gg'\right] - A_2^* M\,\mathrm{Re}\left(\frac{1}{1+m^2}\left(f''-mg'\right)-f''\right) = 0. \tag{4.18}$$

$$Sq\left[\left(g+\frac{1}{2}\eta g'\right)A_1 + 2\left(f'g - fg'\right)\right] = \frac{A^*}{2B^*}g'' - \frac{A_2^*\,\mathrm{Re}\, M}{2B^*}\left[\left(\frac{1}{1+m^2}\right)\left(g+mf'\right)+g\right]. \tag{4.19}$$

$$\frac{\mathrm{Re}}{2\rho_f}p^{*'} = Sq\left(f+\eta f'\right) - 2B\,\mathrm{Re}\, ff' + A^* f'', \tag{4.20}$$

$$\left[\frac{D^*}{\Omega_1 C^*}+Rd\left(1+\left(\frac{1}{\theta_w+s}\right)\theta\right)^3\right]\theta''$$
$$+\left[3Rd\left(1+\left(\frac{1}{\theta_w+s}\right)\theta\right)^2\left(\frac{1}{\theta_w+s}\right)\right]\theta'^2 \tag{4.21}$$

$$-2Sq\,\mathrm{Pr}\,C^*\left[\begin{array}{c} A_1(s+\theta)+\frac{1}{2}\eta\theta'+f'\left(s+\theta+\frac{1}{2}\eta\theta'\right)-2f\theta' \\ +\gamma\left(\begin{array}{c} A_1\left(2(s+\theta+\frac{1}{2}\eta\theta')+\frac{1}{4}\left(3\eta\theta'+\eta^2\theta"\right)\right) \\ +\left(f'+\frac{1}{2}\eta f'\right)(s+\theta)+2\left(s+\theta+\frac{1}{2}\eta\theta'\right) \\ -4f\left(\frac{3}{2}\theta'+\frac{\eta}{2}\theta"\right)+\left(f+\eta f'\right)\theta' \\ +\frac{1}{A_1}f'^2(s+\theta)-\frac{2}{A_1}ff"(s+\theta) \\ -\frac{4}{A_1}f^2\theta'-\left(\frac{4}{A_1}ff'\theta'+\frac{4}{A_1}f^2\theta"\right) \\ +\frac{2}{A_1}\left(s+\theta+\frac{1}{2}\eta\theta'\right)-\frac{4}{A_1}f\left(\frac{1}{2}\eta\theta"+\frac{3}{2}\theta'\right)\end{array}\right)\end{array}\right]$$
$$+\frac{1}{\mathrm{Pr}\,C^*}\left[A_3f'+B_3\theta\right] = 0, \tag{4.22}$$

With boundary conditions:

$$\begin{aligned} f(0) &= 0,\ f(1)=0,\quad f'(0)=\gamma_1,\ f'(1)=\gamma_2, g(0)=1, \\ g(1) &= \Omega, \theta(0)=1-s, \theta(1)=0, P(0)=0. \end{aligned} \tag{4.23}$$

The saturation magnetization parameter is denoted by M. The unsteadiness parameter is A_1, the lower and upper disks scale stretching parameters are γ_1&γ_2 and Pr is the Prandtl number. Ω is the parameter for rotation. The symbol m stands for hall current, thermal relaxation time parameter γ. The parameters of thermal radiation and thermal stratification are represented by Rd and s, respectively. The squeezing variable is Sq. Re stands for Reynold's number. $\theta_w$is the temperature ratio parameter. Temperature and space heat generation/absorption parameters are A_3 and B_3 respectively.

$$\begin{aligned} M &= \frac{\sigma_f B_o^2(1-ct)}{\rho_f(1+m^2)}, A_1=\frac{c}{\Omega_1}, \gamma_1=\frac{a_1}{\Omega_1}, \gamma_2=\frac{a_2}{\Omega_2}, \mathrm{Pr}=\frac{\nu_f(\rho C_P)_f}{k_f}, \\ \Omega &= \frac{\Omega_2}{\Omega_1}, \gamma=\frac{c\epsilon 1}{1-ct}, Rd=\frac{-16\sigma^* T_2^3}{3k_f k^*}, s=\frac{B'}{A'}, Sq=\frac{ch^2}{2\upsilon_f}. \end{aligned} \tag{4.24}$$

4.2 surface drag force coefficient and rate of heat transfer

Shear stress in the radial and tangential directions τ_{zr} and $\tau_{z\theta}$ at lower disk are:

$$\begin{aligned} \tau_{zr} &= \mu_{hnf} u_z|_{z=0} = \frac{\mu_f r\Omega_1 f''(0)}{h(1-\phi)^{2.5}}, \\ \tau_{z\theta} &= \mu_{hnf} u_z|_{z=0} = \frac{\mu_f r\Omega_1 g^{'}(0)}{h(1-\phi)^{2.5}}, \end{aligned} \tag{4.25}$$

The combined shear stress is given by:

$$\tau_w = (\tau_{zr^2} + \tau_{z\theta^2})^{1/2}, \tag{4.26}$$

The components of surface drag force coefficients at lower and upper disks are:

$$C_{f_1} = \frac{\tau_w|_{z=0}}{\rho_{hnf}(r\Omega_1)^2} = \frac{1}{\mathrm{Re}(1-\phi_1)^{2.5}(1-\phi_2)^{2.5}} \left[\left(f''(0)\right)^2 + \left(g'(0)\right)^2 \right]^{1/2}, \tag{4.27}$$

$$C_{f_2} = \frac{\tau_w|_{z=h}}{\rho_{hnf}(r\Omega_2)} = \frac{1}{\mathrm{Re}(1-\phi_1)^{2.5}(1-\phi_2)^{2.5}} \left[\left(f''(1)\right)^2 + \left(g'(1)\right)^2 \right]^{1/2}, \tag{4.28}$$

Here, the local Reynolds number is Re.

Heat transfer rate for both disks are:

$$\begin{aligned} N_{u_{x1}} &= \frac{hq_w}{k_{hnf}(T_1 - T_0)}|_{z=0}. \\ N_{u_{x1}} &= \frac{hq_w}{k_{hnf}(T_1 - T_0)}|_{z=h}. \end{aligned} \tag{4.29}$$

Where q_w is the wall heat flux.

$$\begin{aligned} q_w|_{z=0} &= -k_{hnf}\frac{\partial T}{\partial z}|_{z=0} + \frac{16\sigma_1^* T_1^3}{3k_1^*}\frac{\partial T}{\partial z}|_{z=0} \\ q_w|_{z=h} &= -k_{hnf}\frac{\partial T}{\partial z}|_{z=h} + \frac{16\sigma_1^* T_1^3}{3k_1^*}\frac{\partial T}{\partial z}|_{z=h} \end{aligned} \tag{4.30}$$

Non-dimensional heat transfer rate are:

$$\begin{aligned}(1-ct)^{1/2}\,Nu_1 &= -\left(\frac{k_{hnf}}{k_f}+\left(Rd\,(1+(\theta_w-1)\,\theta\,(0))^3\right)\right)\theta'\,(0)\,.\\ (1-ct)^{1/2}\,Nu_2 &= -\left(\frac{k_{hnf}}{k_f}+\left(Rd\,(1+(\theta_w-1)\,\theta\,(1))^3\right)\right)\theta'\,(1)\,. \end{aligned} \tag{4.31}$$

4.3 Results and discussions

This section focuses on a graphical and tabular study of physical parameters that influence the behaviour of axial velocity $f\,(\eta)$, radial velocity $f\,'\,(\eta)$, Tangential velocity $g(\eta)$, and thermal profile $\theta\,(\eta)$,drag coefficient, and heat transfer rate for various values of the relevant parametres.Impacts of parameters *i.e.*, saturation magnetization parameter M, unsteadiness parameter A_1,squeezing parameter S_q,Scale stretching parameters γ_1&γ_2 Prandtl number Pr,Ω rotation parameter. thermal relaxation time parameter γ, thermal radiation parameter R_d, thermal stratification parameter s,volume fraction coefficient ϕ_1& ϕ_2,temperature ratio coefficient θ_w and Reynolds number Re .We pick two types of volume fractions of nanoparticles, such as ϕ_1 for copper(Cu) and ϕ_2 for Gold(Au).we set the parameters with ranges to attain the desired results:$0 \leq M \leq 2.1, 0.0 \leq A_1 \leq 2.4, 0.0 \leq \gamma_1 \leq 0.4, 0.0 \leq \gamma_2 \leq 2.7, 0.0 \leq \gamma \leq 1, 0.0 \leq \Omega \leq 2, 6.4 \leq \mathrm{Pr} \leq 6.9, 0.0 \leq m \leq 2.4, 0.03 \leq \phi_1 \leq 0.06, 0.0 \leq 2.6, 0.0 \leq 0.3, 0.2 \leq R_d \leq 0.6,$

$0.03 \leq \phi_2 \leq 0.06$.To see the impact of nanoparticle volume friction, results are sketched in Figs. 4.2-4.3. In the presence of Au and Cu as nanoparticles, it is remarked that the axial velocity $f(\eta)$ reduces in some ares close to the disk for growing values of nanoparticle volume friction but after a certain distance from the disk, this profile starts developing until the far-field boundary condition is asymptotically satisfied. We observed the increasing behaviour in Fig. 4.3 for radial velocity $f'(\eta)$.The stretching rate parameter of the lower disk is depicted in Figs. 4.4-4.5 for axial velocity and radial velocity. The axial velocity increases as the rate parameter values are increased, as seen in Fig. 4.4. This behaviour can be observed all around the system. The velocity of the upper disk is $0.2\left(\sec^{-1}\right)$, which is higher than the lower disk's $0.1\left(\sec^{-1}\right)$, causing the $f'(\eta)$ to grow near the disk at z=0 and decreasing in the area of the disk at z =h, as seen in Fig. 4.5.Figs. 4.6-4.7showing the trend of axial and radial velocities for stretching rate parameter of upper disk. At near the lower disk axial $f\,(\eta)$and radial f

$'(\eta)$ velocities decreases in the entire system. But at near the upper disk radial velocity $f'(\eta)$ behaves oppositvely,it shows that disk's increased stretching rate at $z = h$. The velocity profile $f'(\eta)$against the squeezing parameter Sq is represented in Fig. 4.8. The velocity increases for disks contraction, i.e., Sq = -1, -2, -3, however the opposite trend has been observed for Sq = 1, 2, 3 when disks are moving far apart.In the case of contraction(sq=-1,-2,-3),the fluid is subjected to a squeezed force, which causes the fluid to move at a faster rate. As a result, velocity increases. When both disks move far apart, a gap forms between them. The fluid moves in the opposite direction to fill this gap, reducing velocity in the radial direction.

Figs. 4.9 sketched for tangential velocity $g(\eta)$ on hybrid nanoparticles volume fraction, by increasing the nanoparticle volume $\phi_1(\eta)$ velocity increases. It is observed that tangential velocity $g(\eta)$ is a decreasing function of Hall parameter m in Fig. 4.10. Reynolds number $R_e = (\rho\nu d/\mu)$ represents the ratio of inertial forces to viscous forces. Increase in Re causes the inertial forces to increase, which slow down the particles movement. Decline in tangential velocity $g(\eta)$ for values of Re can be seen in Fig. 4.11. Fig. 4.12 shows the effect of magnetic parameter M on tangential velocity of hybrid nanofluid. It is noted that increasing the magnetic field parameter M causes reduction in tangential velocity $g(\eta)$, which is shown in Fig. 4.12. Actually, the magnetic parameter M depends on magnetic field strength which creates the Lorentz force. Thus increasingthe magnetic field parameter M implies increase in Lorentz force (resistive force), which produces friction between the surface and fluid that causes a decrease in tangential velocity. Rotation parameter is defined as $\Omega = \frac{\Omega_2}{\Omega_1}$. As both a result, it is evident that increased angular velocity indicates a high rotation rate, and so the rotation rate becomes higher than the stretching rate. Physically, increasing the rotation parameter raises the centrifugal force, which in turn exerts pressure on the fluid, causing the fluid particles to move more quickly. Fig. 4.13 shows that $g(\eta)$ is increasing as a function of Ω.

The features of radiation parameter Rd on hybrid nanofluid temperature profile $\theta(\eta)$ are deployed in Fig. 4.14. It is illustrated that increasing amount of radiation parameter Rd gained more heat to the nanofluid which causes to enhance temperature profile. Physically, inclusion of radiation in temperature field cause to enhance Brownian movement in molecular level. Also continuous collision of tiny nanoparticles will generally gain more heat and thus result in an enhancement in the fluid temperature. For the thermal relaxation parameter γ,

the thermal profile $\theta(\eta)$ of squeezing hybrid nanofluid is seen in Fig. 4.15. It shows that as the thermal relaxation parameter rate rises, the thermal profile rises as well. The thickness of the thermal boundary layer decreases as the value of the relaxation parameter increases. Fig. 4.16 displays the impact of Prandtl number Pr on temperature profile $\theta(\eta)$. Physically, Pr is defined as "the ratio of momentum diffusivity to thermal diffusivity". So an increasing variation of Pr implies the smaller value of thermal diffusivity which actually leads to reduction in the temperature of fluid. Physically, the increase in Prandtl number Pr shows that the heat penetration depth becomes thinner. The hybrid nanofluid is more efficient for heat transport, while cooling procedure will be more proficient for usual nanofluid. Fig. 4.17 demonstrates that increasing the value of thermal startification parameter s causes to decline in temperature profile. Fig. 4.18 shows the effect of the temperature ratio parameter on temperature profile. It indicates that raising θ_w improves temperature and the thickness of the thermal boundary layer. When Sq -0.1,-0.5,-0.9 i.e., when the disks are contracting, the temperature exhibits a lowering behaviour, as shown in Fig. 4.19. However, at larger values of the squeezing parameter $Sq = 0.1,0.5,0.9$ (i.e. when the disks are moving far apart), it shows a rising trend.Temperature profile $\theta(\eta)$ for A_3 and B_3 values are shown in Figs. 4.20-4.23. It is clear from these graphs that as the A_3 and B_3 values rise, the temperature profiles rise as well. Because of non-uniform heat generation, the temperature of hybrid nanofluid is dramatically raised. Higher non-uniform heat generation estimates generate more heat, which finally raises the fluid temperature.It is clear from these graphs that as the A_3 and B_3 rise towards negative values, the temperature profiles falls. Because of non-uniform heat absorption, the temperature of hybrid nanofluid is dramatically decreased. Higher non-uniform heat absorption estimates absorb more heat, which finally decreases the fluid temperature

Table 4.2 shows the effects of the Reynolds number Re, Hartman number M, Hall effect and stretching parameters γ_1 and $\gamma_2$on skin friction coefficients at the lower and upper discs. For larger values of Re, M, m, γ_1 and γ_2, the skin friction coefficient increases at the bottom disc. The skin friction coefficient at the upper disc is improved by increasing the values of Re, M, m, γ_1 and γ_2. The effect of the thermal stratification parameter s, the Prandtl number Pr, and the radiation parameter Rd on the rate of heat transfer between the lower and upper discs is shown in Table 4.3. At both discs, the effect of Pr on Nusselt number is observed to

be opposite. Nusselt number decreases as Pr grows on the lower disc, while it increases on the top disc. The heat transfer rate at both discs reduces as the value of s is increased. The heat transfer rate at both discs increases as the radiation parameter Rd is increased.

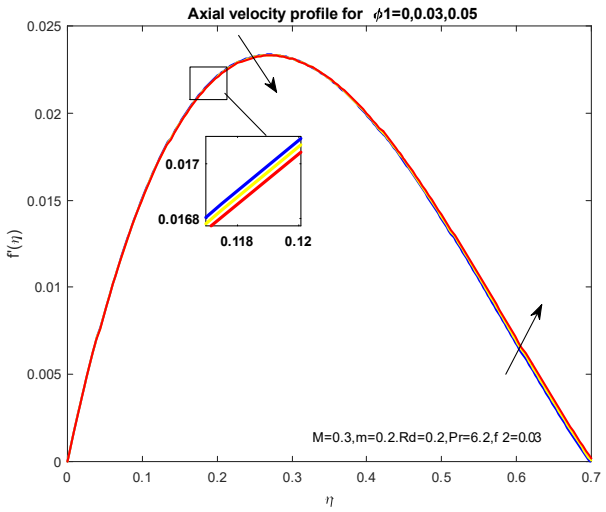

Fig. 4.2 Change in $f(\eta)$ vs.ϕ_1

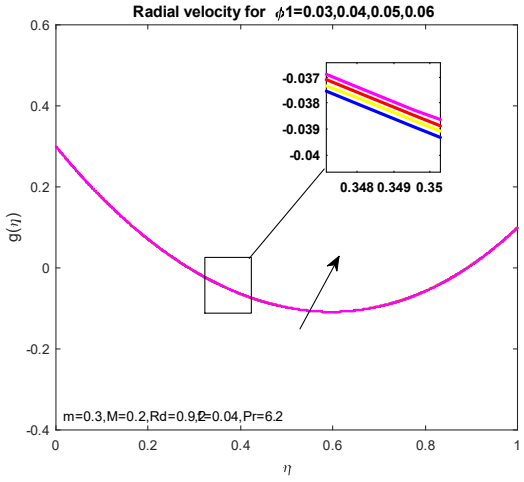

Fig.4.3 Change in $f'(\eta)$ vs.ϕ_1

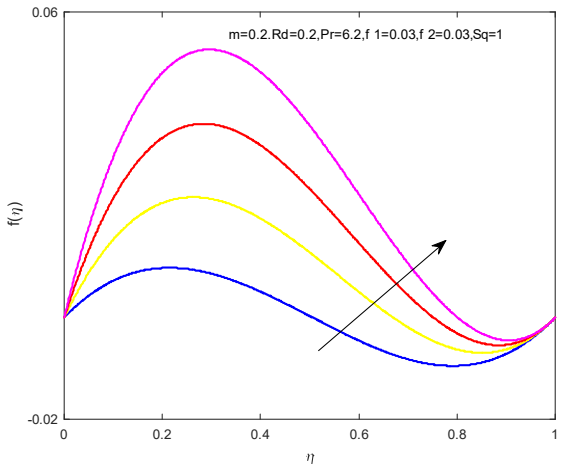

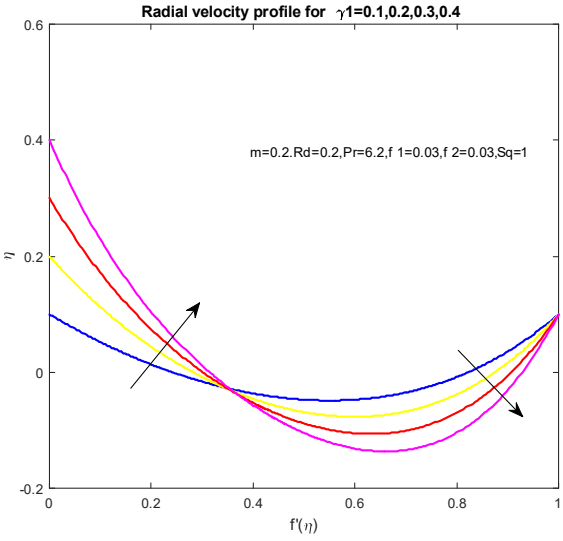

Fig.4.5 Change in $f'(\eta)$ vs.γ_1

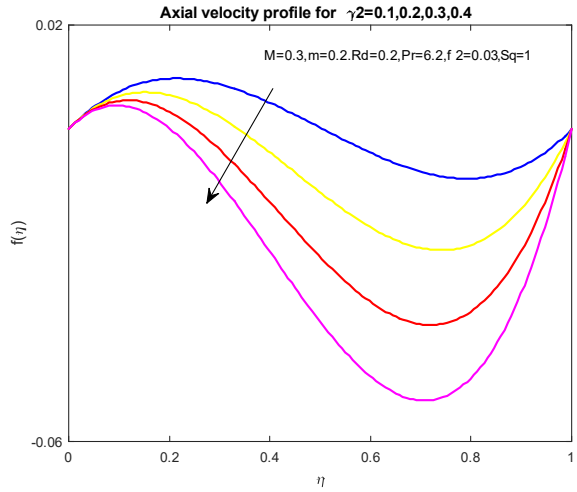

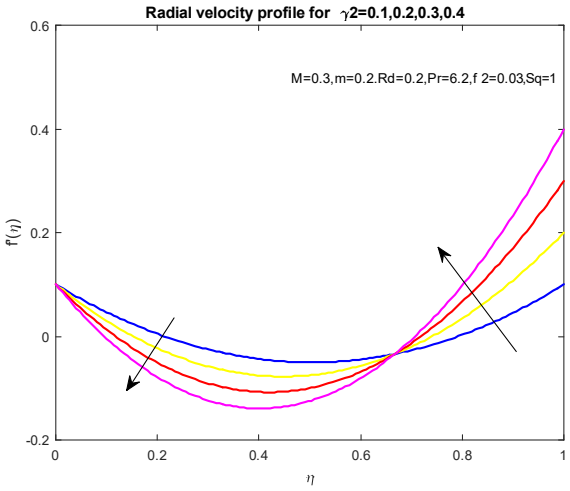

Fig. 4.7 Change in $f'(\eta)$ vs.γ_2

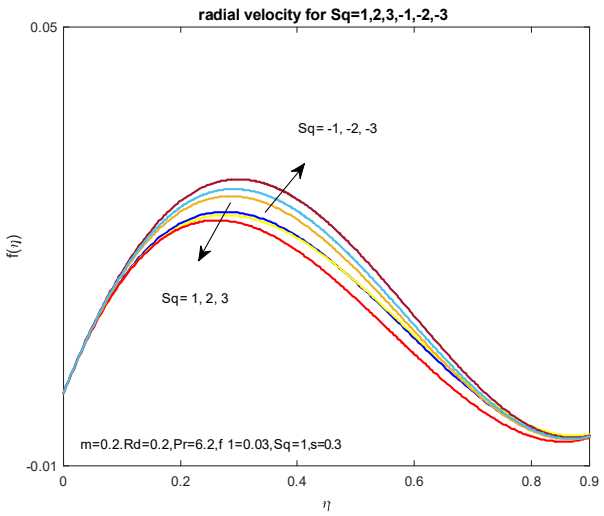

Fig. 4.8 Change in $f'(\eta)$ vs.Sq

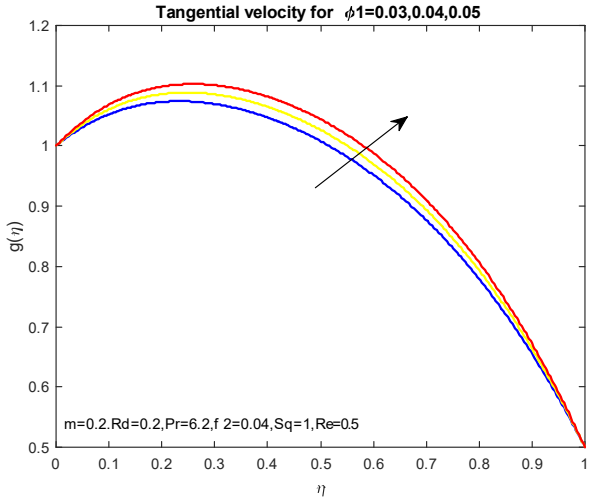

Fig. 4.9 Change in $g(\eta)$ vs.ϕ_1

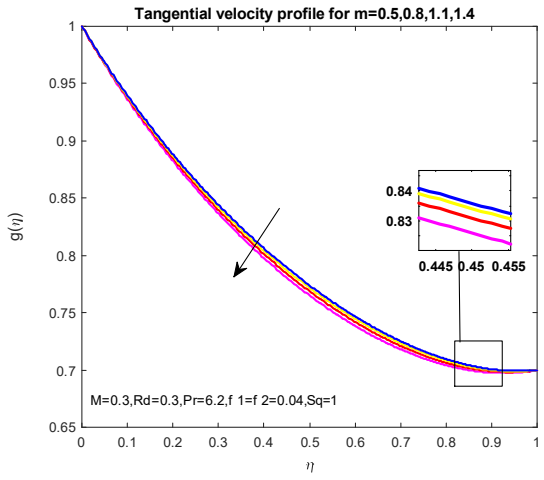

Fig. 4.10 Change in $g(\eta)$ vs.m

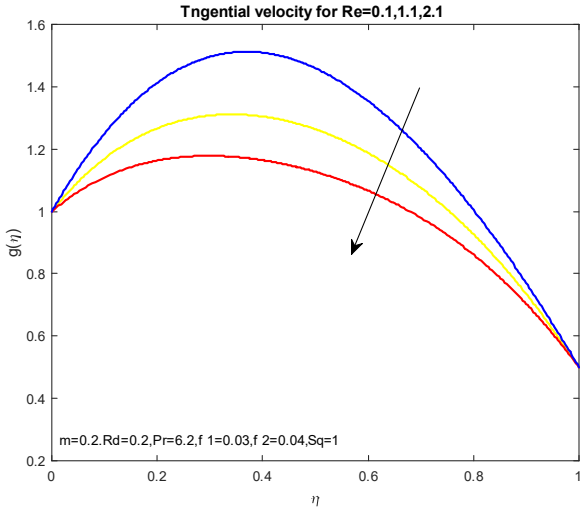

Fig. 4.11 Change in $g(\eta)$ vs.Re

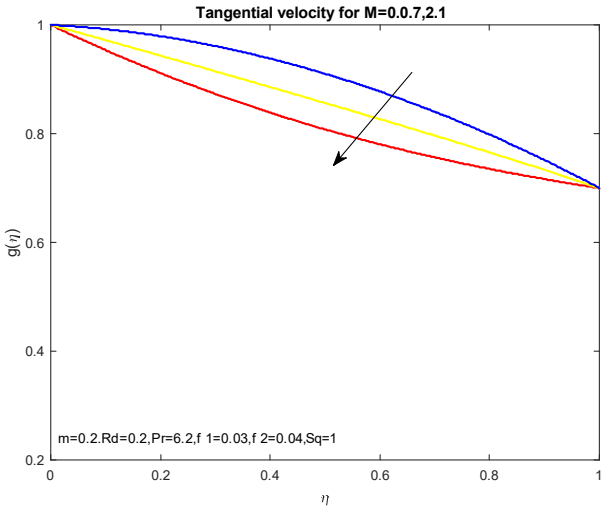

Fig. 4.12 Change in $g(\eta)$ vs.M

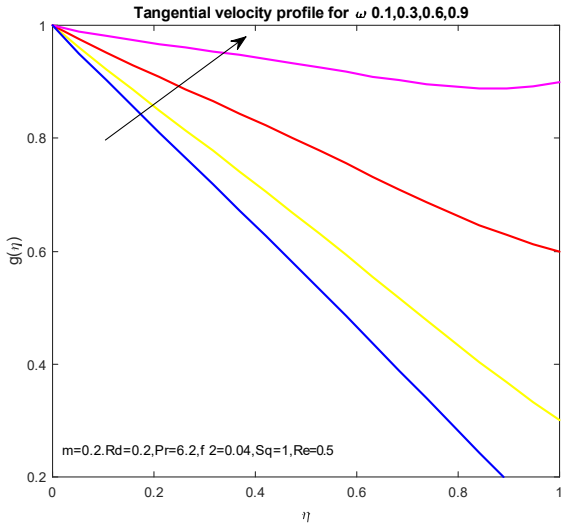

Fig. 4.13 Change in $g(\eta)$ vs.Ω

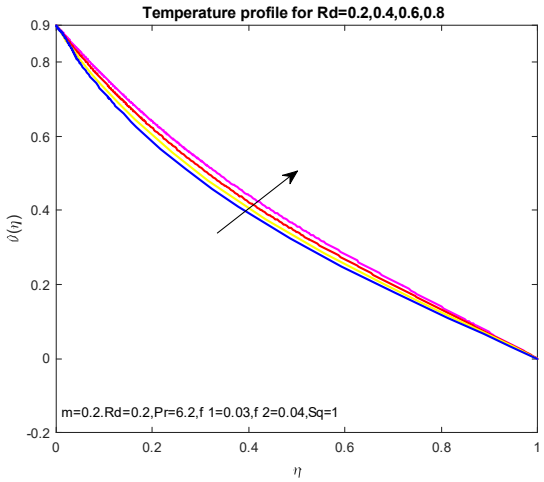

Fig. 4.14 Change in $\theta(\eta)$ vs.Rd

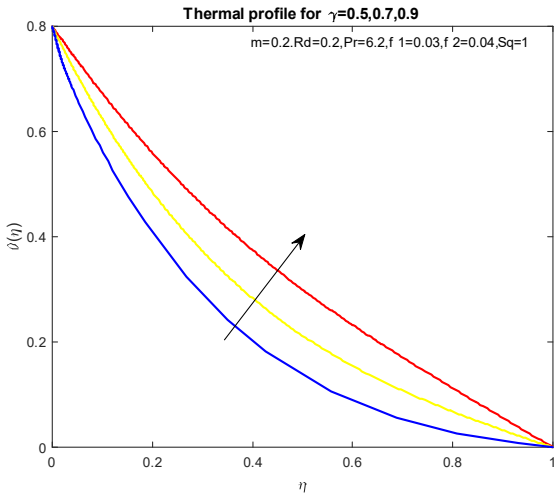

Fig.4.15 Change in $\theta(\eta)$ vs.γ

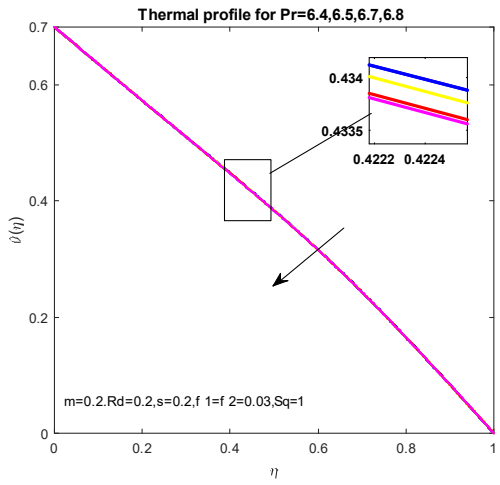

Fig. 4.16 Change in $\theta(\eta)$ vs.Pr

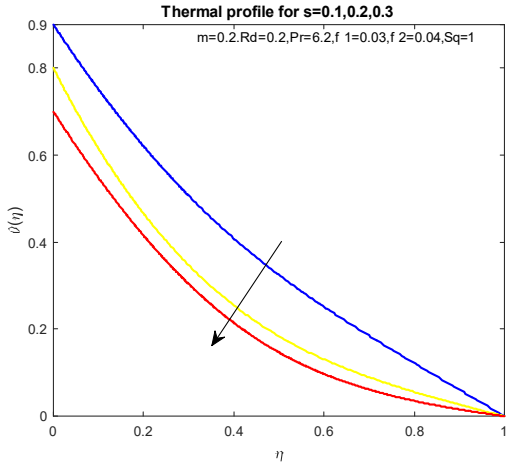

Fig. 4.17 Change in $\theta(\eta)$ vs.s

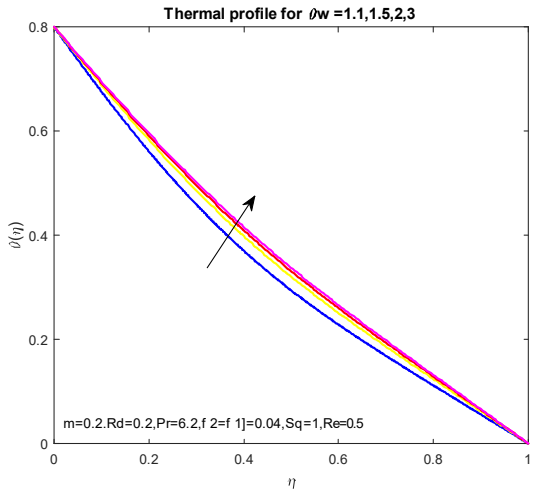

Fig. 4.18 Change in $\theta(\eta)$ vs.θ_w

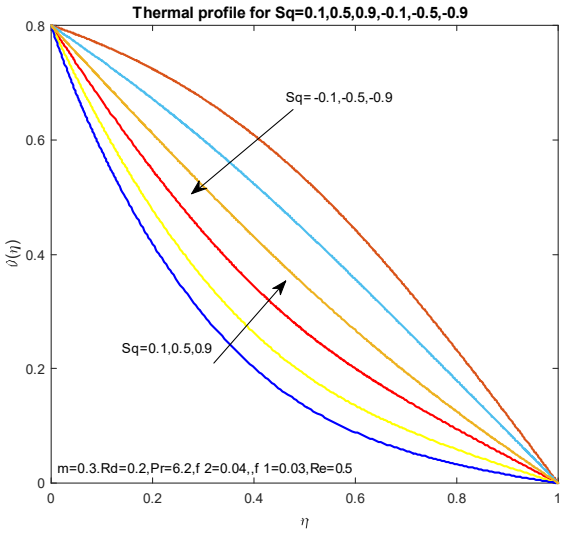

Fig. 4.19 Change in $\theta(\eta)$ vs.Sq

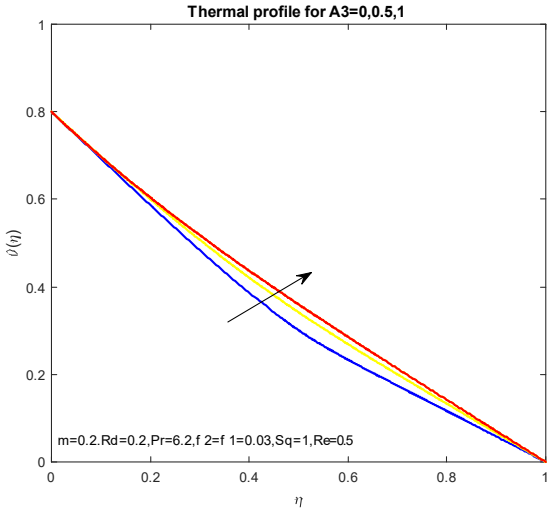

Fig. 4.20 Change in $\theta(\eta)$ vs.A_3

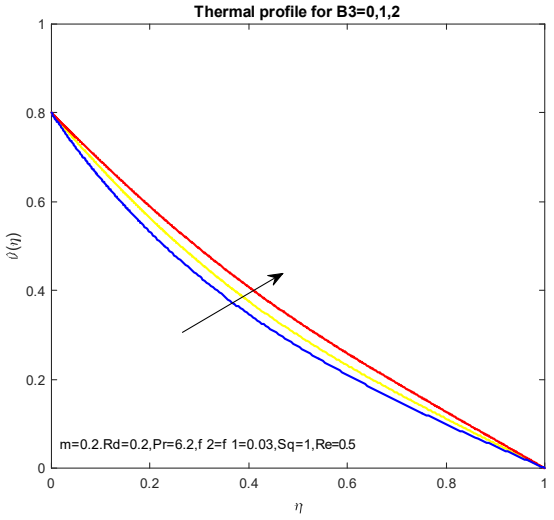

Fig.4.21 Change in $\theta(\eta)$ vs.B_3

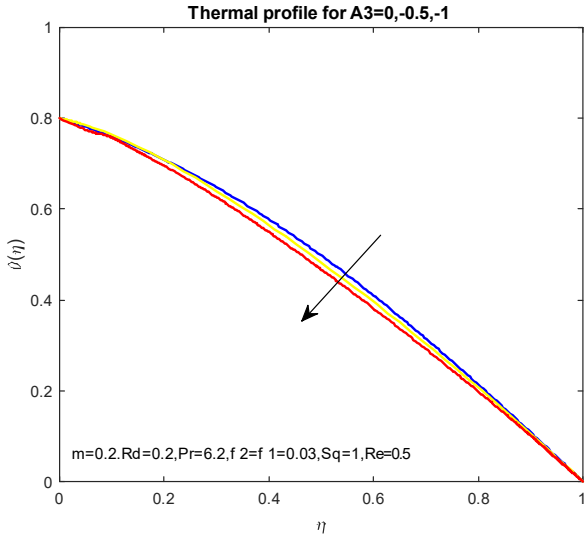

Fig.4.22 Change in $\theta(\eta)$ vs.A_3

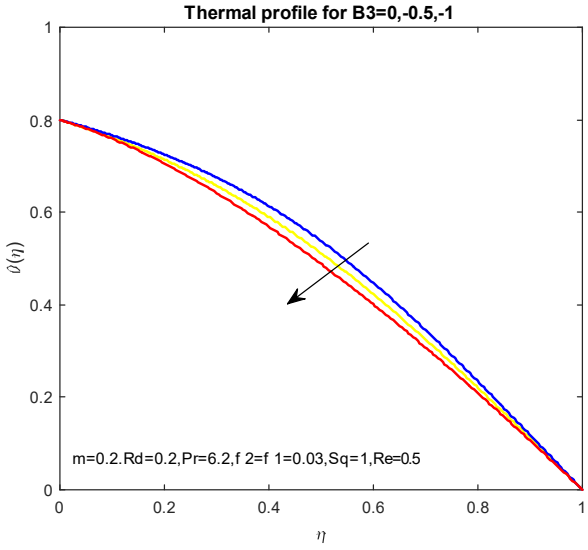

Fig.4.23 Change in $\theta(\eta)$ vs.B_3

Table 4.2 Numerical values of Skin friction coefficient for upper and lower discs when. $A_1 = 0.5, \mathrm{Pr} = 6.7, \Omega = 0.5, s = 0.4$

m	M	Re	γ_1	γ_2	C_1	C_2
0	0				1.2457	-0.7285
	0.5				1.2474	-0.5454
0.5	0				1.9581	-0.7285
	0.5				1.6156	-0.5915
	1				1.1779	-0.4612
1	0.5	0.5			1.1536	-0.6262
		1			0.9246	-0.5340
		1.5			0.5078	-0.4427
			0.1		0.8033	-0.4427
			0.2		0.5078	-0.5337
			0.1	0.2	0.6738	-0.4427
				0.4	3.5940	-0.6456

Table 4.3 Numerical values of heat transfer rate for upper and lower discs when.

$A_1 = 0.5, \Omega = 0.5$

s	Pr	Rd	C_1	C_2
0.2			-3.64274	-3.64374
0.4			-2.71601	-2.73601
0.6			-1.81602	-1.82602
0.2			-3.63374	-3.64374
	6.7		-3.63437	-3.64374
	6.8		-3.63314	-3.64374
	6.9	0.5	-3.63314	-3.63324
		0.6	-3.62276	-3.62276
		0.7	-3.61276	-3.61176

Chapter 5

Conclusions and future work

We studied two problems in this thesis. First one is review work whille other is extended work. Conclusions for both problems are as follows:

5.1 Chapter 3

- Nonlinear thermal radiation has a growing effect on the heat transfer profile of multi($MWCNTs$) and single($SWCNTs$) wall carbon nanotubes.
- The thermal profile rises as the thermal relaxation time rises.
- For escalating nanoparticle volume fraction, radial velocity and thermal profiles are growing.
- Tangential velocity increases as Ω increases.

5.2 Chapter 4

- For Sq radial $g(\eta)$ and temperature $\theta(\eta)$ profiles have a two-fold behaviour: when disks contract, the profiles increases and when disks move far apart, the profiles decreases.
- Tangential velocity is found to be a falling factor of Hall parameter m.
- Volume fraction of nanoparticles ϕ has enhancing impact on Radial $f'(\eta)$ and Tangential $g(\eta)$ velocities.

- The fluid temperature $\theta(\eta)$ improving for growing values of temperature ratio coeffcient θ_w.
- The fluid temperature $\theta(\eta)$ falls for growing values of Prandtl number Pr due to smaller thermal diffusivity.
- The axial velocity $f(\eta)$ is rising for growing values of stretching rate parameter of the lower disk γ_1 while for stretching rate parameter of upper disk γ_2 it drops.
- It is noticed that dimensionless temperatuer $\theta(\eta)$ increases for non-uniform heat generation parameter.

5.3 Future work

- The present work may be extended to the following:
- Any other non-Newtonian fluid along with appropriate boundary conditions.
- Bio-convective nano-fluid with microorganisms.
- Boundary conditions also be changed to second order slip.
- Flow over curve surface with activation energy.

Bibliography

[1] Das SK, Choi SU, Patel HE (2006) Heat transfer in nanofluids—a review. Heat transfer engineering 27 (10):3-19

[2] Saidur R, Leong K, Mohammed HA (2011) A review on applications and challenges of nanofluids. Renewable and sustainable energy reviews 15 (3):1646-1668

[3] Suganthi K, Rajan K (2017) Metal oxide nanofluids: Review of formulation, thermophysical properties, mechanisms, and heat transfer performance. Renewable and Sustainable Energy Reviews 76:226-255

[4] Ali N, Teixeira JA, Addali A (2018) A Review on Nanofluids: Fabrication, Stability, and Thermophysical Properties. Journal of Nanomaterials 2018:6978130. doi:10.1155/2018/6978130

[5] Sarkar J, Ghosh P, Adil A (2015) A review on hybrid nanofluids: recent research, development and applications. Renewable and Sustainable Energy Reviews 43:164-177

[6] Keblinski P, Eastman JA, Cahill DG (2005) Nanofluids for thermal transport. Materials today 8 (6):36-44

[7] Masuda H, Ebata A, Teramae K (1993) Alteration of thermal conductivity and viscosity of liquid by dispersing ultra-fine particles. Dispersion of Al2O3, SiO2 and TiO2 ultra-fine particles.

[8] Lee S, Choi S-S, Li S, and, Eastman J (1999) Measuring thermal conductivity of fluids containing oxide nanoparticles.

[9] Das SK, Putra N, Thiesen P, Roetzel W (2003) Temperature dependence of thermal conductivity enhancement for nanofluids. J Heat Transfer 125 (4):567-574

[10] Babu JR, Kumar KK, Rao SS (2017) State-of-art review on hybrid nanofluids. Renewable and Sustainable Energy Reviews 77:551-565

[11] Das SK, Choi SU, Patel HE (2006) Heat transfer in nanofluids—a review. Heat transfer engineering 27 (10):3-19

[12] Saidur R, Leong K, Mohammed HA (2011) A review on applications and challenges of nanofluids. Renewable and sustainable energy reviews 15 (3):1646-1668

[13] Suganthi K, Rajan K (2017) Metal oxide nanofluids: Review of formulation, thermophysical properties, mechanisms, and heat transfer performance. Renewable and Sustainable Energy Reviews 76:226-255

[14] Ali N, Teixeira JA, Addali A (2018) A Review on Nanofluids: Fabrication, Stability, and Thermophysical Properties. Journal of Nanomaterials 2018:6978130. doi:10.1155/2018/6978130

[15] Sarkar J, Ghosh P, Adil A (2015) A review on hybrid nanofluids: recent research, development and applications. Renewable and Sustainable Energy Reviews 43:164-177

Keblinski P, Eastman JA, Cahill DG (2005) Nanofluids for thermal transport. Materials today 8 (6):36-44

[16] Masuda H, Ebata A, Teramae K (1993) Alteration of thermal conductivity and viscosity of liquid by dispersing ultra-fine particles. Dispersion of Al2O3, SiO2 and TiO2 ultra-fine particles.

[17] Lee S, Choi S-S, Li S, and, Eastman J (1999) Measuring thermal conductivity of fluids containing oxide nanoparticles.

[18] Das SK, Putra N, Thiesen P, Roetzel W (2003) Temperature dependence of thermal conductivity enhancement for nanofluids. J Heat Transfer 125 (4):567-574

[19] Babu JR, Kumar KK, Rao SS (2017) State-of-art review on hybrid nanofluids. Renewable and Sustainable Energy Reviews 77:551-565

[20] Eastman JA, Choi U, Li S, Thompson L, Lee S (1996) Enhanced thermal conductivity through the development of nanofluids. Argonne National Lab., IL (United States),

[21] Xie H, Wang J, Xi T, Liu Y, Ai F, Wu Q (2002) Thermal conductivity enhancement of suspensions containing nanosized alumina particles. Journal of applied physics 91 (7):4568-4572

[22] Biercuk M, Llaguno MC, Radosavljevic M, Hyun J, Johnson AT, Fischer JE (2002) Carbon nanotube composites for thermal management. Applied physics letters 80 (15):2767-2769

[23] Choi S, Zhang ZG, Yu W, Lockwood F, Grulke E (2001) Anomalous thermal conductivity enhancement in nanotube suspensions. Applied physics letters 79 (14):2252-2254

[24] Evans W, Fish J, Keblinski P (2006) Role of Brownian motion hydrodynamics on nanofluid thermal conductivity. Applied Physics Letters 88 (9):093116

[25] Xuan Y, Li Q (2000) Heat transfer enhancement of nanofluids. International Journal of heat and fluid flow 21 (1):58-64

[26] Madhesh D, Parameshwaran R, Kalaiselvam S (2014) Experimental investigation on convective heat transfer and rheological characteristics of Cu–TiO2 hybrid nanofluids. Experimental Thermal and Fluid Science 52:104-115

[27] Nimmagadda R, Venkatasubbaiah K (2015) Conjugate heat transfer analysis of microchannel using novel hybrid nanofluids (Al2O3+ Ag/Water). European Journal of Mechanics-B/Fluids 52:19-27

[28] Madhesh D, Kalaiselvam S (2014) Experimental analysis of hybrid nanofluid as a coolant. Procedia engineering 97:1667-1675

[29] Takabi B, Salehi S (2014) Augmentation of the heat transfer performance of a sinusoidal corrugated enclosure by employing hybrid nanofluid. Advances in Mechanical Engineering 6:147059

[30] Stefen M (1874) Versuch Uber die scheinbare adhesion. Sitzungsberichte der Akademie der Wissenschaften in Wien Mathematik-Naturwissen 69:713-721

[31] Muhammad K, Hayat T, Alsaedi A, Ahmad B (2020) Melting heat transfer in squeezing flow of basefluid (water), nanofluid (CNTs+ water) and hybrid nanofluid (CNTs+ CuO+ water). Journal of Thermal Analysis and Calorimetry:1-18

[32] Siddiqui AM, Irum S, Ansari AR (2008) Unsteady squeezing flow of a viscous MHD fluid between parallel plates, a solution using the homotopy perturbation method. Mathematical Modelling and Analysis 13 (4):565-576

[33] Domairry G, Aziz A (2009) Approximate analysis of MHD squeeze flow between two parallel disks with suction or injection by homotopy perturbation method. Mathematical Problems in Engineering 2009

[34] Mustafa M, Hayat T, Obaidat S (2012) On heat and mass transfer in the unsteady squeezing flow between parallel plates. Meccanica 47 (7):1581-1589

[35] Sarojamma G, Mahaboobjan S, Sreelakshmi K (2015) Effect of Hall current on the flow induced by a stretching surface. IJSIMR 3 (3):1139-1148

[36] Makinde O, Iskander T, Mabood F, Khan W, Tshehla M (2016) MHD Couette-Poiseuille flow of variable viscosity nanofluids in a rotating permeable channel with Hall effects. Journal of Molecular liquids 221:778-787

[37] Iqbal Z, Akbar NS, Azhar E, Maraj EN (2018) Performance of hybrid nanofluid (Cu-CuO/water) on MHD rotating transport in oscillating vertical channel inspired by Hall current and thermal radiation. Alexandria Engineering Journal 57 (3):1943-1954. doi:https://doi.org/10.1016/j.aej.2017.03.047

[38] Khan M, Ali W, Ahmed J (2020) A hybrid approach to study the influence of Hall current in radiative nanofluid flow over a rotating disk. Applied Nanoscience 10:5167-5177

[39] Gul N, Ramzan M, Chung JD, Kadry S, Chu Y-M (2020) Impact of hall and ion slip in a thermally stratified nanofluid flow comprising Cu and Al 2 O 3 nanoparticles with nonuniform source/sink. Scientific Reports 10 (1):1-18

[40] Borah A, Pati S (2021) Influence of non-uniform asymmetric heating on conjugate heat transfer in a rectangular minichannel using nanofluid by two-phase Eulerian-Lagrangian method. Powder Technology 381:164-180

[41] Koriko OK, Animasaun IL, Omowaye AJ, Oreyeni T (2019) The combined influence of nonlinear thermal radiation and thermal stratification on the dynamics of micropolar fluid along a vertical surface. Multidiscipl. Model. Mater. Struct.

Maham Thesis

ORIGINALITY REPORT

0%	0%	0%	%
SIMILARITY INDEX	INTERNET SOURCES	PUBLICATIONS	STUDENT PAPERS

PRIMARY SOURCES

Exclude quotes	On	Exclude matches	< 5 words
Exclude bibliography	On		